Photo-driven effects in twist-bend nematic phases: dynamic and memory response of liquid crystalline dimers.

Daniel Zaton,[a, b] Alexia Karamoula,[a] Grant J. Strachan,[b] John M.D. Storey,[b] Corrie T. Imrie,[b] and Alfonso Martinez-Felipe[a, c,†]

Abstract

We apply UV light to control the stability of twist-bend nematic phases, N_{TB}, and conventional nematic phases, N, in three new liquid crystalline nonsymmetric dimers containing cyanobiphenyl and light-responsive azobenzene fragments connected by a hexyloxy spacer. The dynamic and static (5 *kHz*) dielectric responses of (E)-4'-(6-(4-((4-(ethoxy)phenyl)diazenyl)phenoxy)hexyl)-[1,1'-biphenyl]-4-carbonitrile, CB6OAzO2, (E)-4'-(6-(4-((4-(hexyloxy)phenyl)diazenyl)phenoxy)hexyl)-[1,1'-biphenyl]-4-carbonitrile, CB6OAzO6, and (E)-4'-(6-(4-((4-hexylphenyl)diazenyl)phenoxy)hexyl)-[1,1'-biphenyl]-4-carbonitrile, CB6OAz6, are measured at different temperatures, in planar and homeotropic alignments, by the application of *bias* and alternating electrical fields. The three CB6OAz(O)*n* dimers show high values of the dielectric mean, $\bar{\varepsilon}$, and dielectric anisotropy, $\Delta\varepsilon$, due to the dipole moment associated with the cyanobiphenyl groups. The absence of the ether linkage to the terminal chain in CB6OAz6 reduces the N_{TB} - N transition temperature and increases the bend elastic constant, K_3, compared to those seen for CB6OAzO6. Isothermal phase transitions are promoted by light-irradiation, *via trans*-to-*cis* photoisomerisation of the azobenzene units, resulting in the disruption of the liquid crystal order and appearance of re-entrant nematic and isotropic phases at low temperatures. It is possible to control the dynamics and reversibility of these transitions by varying the chemical structure of the new dimers, the temperature and UV light dosage. This may be exploited in devices using multiple external stimuli.

[a] Chemical and Materials Engineering Group, School of Engineering, King's College, University of Aberdeen, Aberdeen, AB24 3UE, UK.

[b] Department of Chemistry, King's College, University of Aberdeen, Aberdeen, AB24 3UE, UK.

[c] Centre for Energy Transition, University of Aberdeen, Aberdeen, AB24 3UE, UK.

*,† Corresponding author: a.martinez-felipe@abdn.ac.uk

1. Introduction

The twist-bend nematic, N_{TB}, phase was predicted first by Meyer in 1976 [1] and then, and independently, by Dozov in 2001,[2] prior to its discovery by Cestari et al. in 2011.[3] The N_{TB} phase can be considered as a generalised case of the chiral nematic phase, N*, and in the N_{TB} phase, the director, *n*, simultaneously twists and bends resulting in nanoscale helical structures. As a result, *n* is tilted at a constant angle $\theta < 90^o$ with respect to the helix axis, **Fig. 1**. The N_{TB} phase is locally chiral, even though it is composed of achiral molecules, and represents the first example of spontaneous chiral symmetry breaking in a fluid system with no long-range positional order. The handedness of the helix forms spontaneously, and so equal numbers of left- and right-handed helices are expected. This degeneracy may be removed by the introduction of molecular chirality, and the chiral twist-bend nematic phase is obtained.[4]

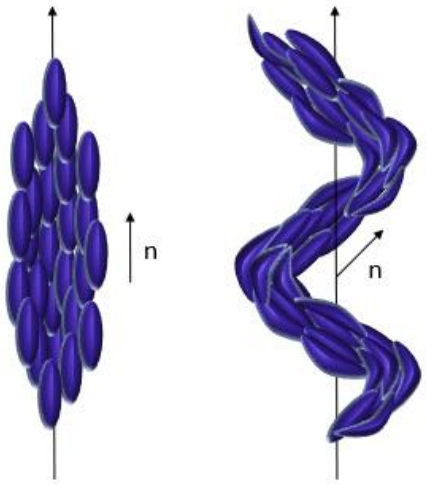

Figure 1. Sketch of the nematic phase, N (left), and the twist-bend nematic phase, N_{TB} (right).

The first compound to unambiguously exhibit the N_{TB} phase was the liquid crystal dimer 1,7-bis(4-cyanobiphenyl-4-yl) heptane , CB7CB, [3]

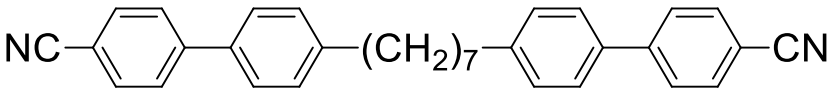

CB7CB

CB7CB is a member of the CB*n*CB series, and has an odd-membered flexible spacer connecting the two cyanobiphenyl mesogenic units. The heptamethylene spacer provides sufficient curvature to drive the helicoidal arrangement of the N_{TB} phase. Although the vast majority of twist-bend

nematogens are odd-membered dimers,[5, 6] a wide variety of other structures also show N_{TB} behaviour, including bent-core molecules,[7] higher oligomers,[8-12] and polymers.[13] In each of these structures bent fragments exist, and this appears to be the structural prerequisite for the observation of the N_{TB} phase. Twist-bend smectic phases, SmC_{TB}, have also been recently discovered.[14, 15]

In addition to the fundamental importance of the N_{TB} phase, it also has very significant application potential. It is possible, for example, to control the spectral response of mixtures containing twist-bend nematogens by switching between light-scattering, colour reflection and transparent states, as a function of electrical fields.[16, 17] The optical properties can be modulated by changing the helicoidal pitch formed by the directors, *via* fast polar switching[18] under the application of variable electrical fields.[19]

Light can also be used as a tool with which to exert spatial control over molecular order in liquid crystals, for example, by utilising the *trans*-to-*cis* photoisomerization of an azobenzene unit. We have systematically investigated twist-bend nematogens containing azobenzene groups,[20-22] and reported the first example of an isothermal and reversible phase transition between the twist-bend nematic, N_{TB}, and the conventional nematic phase, N, by irradiation using actinic UV light (~365 nm) for the nonsymmetric dimer E)-4'-(6-(4-((4-(butoxy)phenyl)diazenyl)phenoxy)hexyl)-[1,1'-biphenyl]-4-carbonitrile, CB6OAzO4, [23]

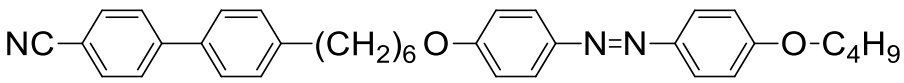

CB6OAzO4

The N_{TB} - N transition was driven by the *trans*-to-*cis* photoisomerisation of the azobenzene unit, which results in the disruption of the helicoidal order together with a six-fold (reversible) increase of its viscoelastic properties.[24, 25] Recently, light irradiation of increasing intensity has been shown to increase the helicoidal pitch in the N_{TB} phase of dimers containing azobenzene groups, up to a threshold value at which the helicoidal arrangements are no longer sustained, resulting in a transition to the conventional nematic phase.[26] Studies of new photosensitive N_{TB} materials, see [27] for a recent example where the mesophase is maintained in a wide range of temperatures, continue in order to understand the underlying mechanisms that will allow us to develop new molecular logic gates, data recording and storage photo-electronic devices, and molecular switches.[28]

In this work, we study the effect of light on the phase behaviour of three new azobenzene-based liquid crystal dimers that show the N_{TB} phase. These nonsymmetric dimers contain cyanobiphenyl, CB, and azobenzene-based, Az, mesogenic units, linked by the odd-membered hexyloxy spacer, -6O-. The azobenzene-based mesogenic unit has either an ethoxy (O2), hexyloxy (O6) or hexyl (6) terminal chain, see **Fig. 2**. Our aim is to investigate the dynamic response to light of these dimers using dielectric analysis, in order to better understand the reported observations made using polarised light microscopy.[23]

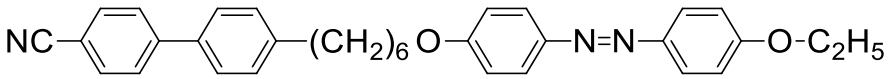

CB6OAzO2

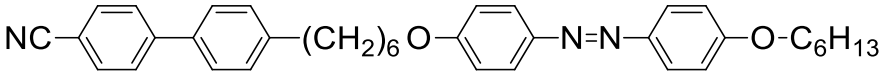

CB6OAzO6

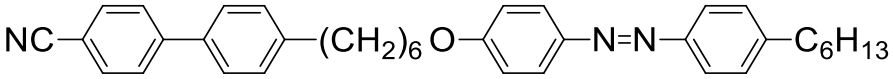

CB6OAz6

Figure 2. The structures of the nonsymmetric dimers and the acronyms used to refer to them.

2. Experimental procedure

Materials synthesis. The synthetic routes to obtain (E)-4'-(6-(4-((4-(ethoxy)phenyl)diazenyl)phenoxy)hexyl)-[1,1'-biphenyl]-4-carbonitrile, CB6OAzO2, (E)-4'-(6-(4-((4-(hexyloxy)phenyl)diazenyl)phenoxy)hexyl)-[1,1'-biphenyl]-4-carbonitrile, CB6OAzO6, and (E)-4'-(6-(4-((4-hexylphenyl)diazenyl)phenoxy)hexyl)-[1,1'-biphenyl]-4-carbonitrile, CB6OAz6, are summarised in **Fig. 3**, and details of the synthetic procedures are included in the supplementary information.

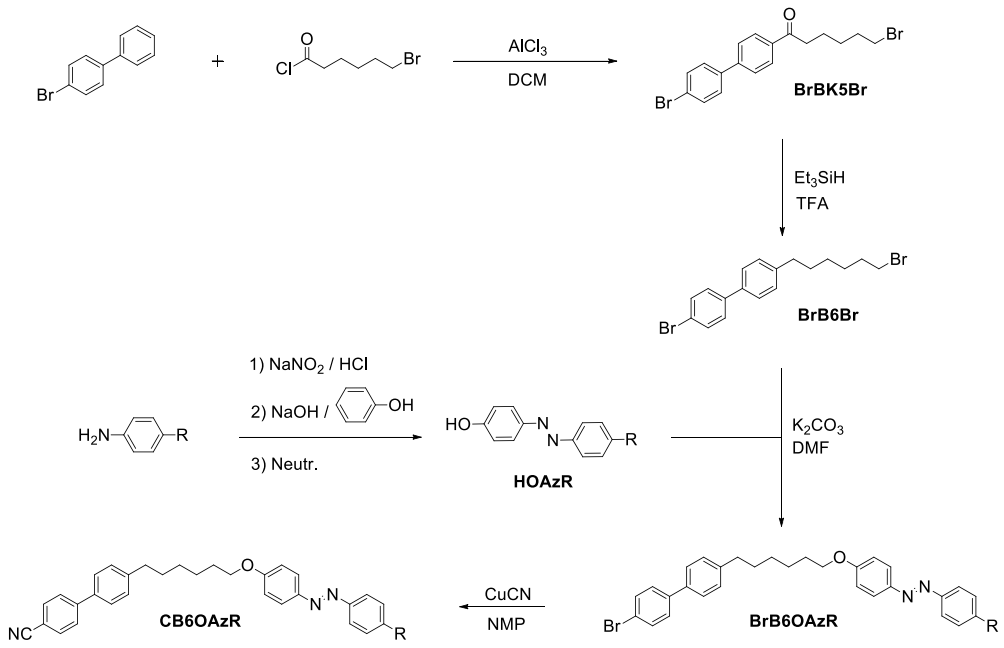

Figure 3. The synthetic pathways used to obtain CB6OAzO2, CB6OAzO6 and CB6OAz6 (R = OC_2H_5, OC_6H_{13} and C_6H_{13}).

Characterisation techniques. Phase identification was carried out by polarised optical microscopy, POM, using an Olympus BH-2 microscope, with temperature controlled by a Linkam THMS 600 heating stage and TMS 91 control unit (± 0.1 K). All the observations obtained by POM used a red colour filter to remove the UV light from the microscope's light source. The thermal transitions were investigated using differential scanning calorimetry, DSC, using a Mettler Toledo DSC821 module, and analysed with the STARe Software. All traces were obtained on heat, cool and reheat cycles with rates of 10 $^{o}C \cdot min^{-1}$ under a nitrogen atmosphere. All samples had a mass between 2 and 10 mg, and the DSC module was calibrated using indium.

Fourier-transform infrared spectra (FT-IR) were obtained using a Thermo Nicolet NEXUS 470 FT-IR spectrometer, and an attenuated total reflectance accessory, ATR, with 4 cm^{-1} resolution, and in the 4000 - 400 cm^{-1} range. Results were taken after 64 scans, and analysed with OMNIC software. UV-vis spectra of the dimers were collected for $\sim 3 \cdot 10^{-5}$ M THF solutions as a function of exposure and relaxation time. Measurements were taken using a VARIAN Cary 50 Scan UV spectrophotometer between 300 nm and 550 nm.

The dielectric response of the dimers was evaluated by complex impedance spectroscopy, using either a Solartron 1260 Impedance/Gain-Phase Analyser, or a Keysight E4980A 2MHz Precision LCR Meter. Indium tin oxide (ITO) cells (SG100A080mG180, Instec), were filled by capillary action with the dimers in the isotropic phase, to yield parallel alignments with 1^{o}-3^{o} pre-tilt angles, as assessed by POM. The cells had active areas of A = 100 mm^2, with 100 Ω resistance, and thickness, $v \sim$ 8 μm. The capacitance of the cell, C_O, was calculated as,

$$C_O = \epsilon_O \frac{A}{v} = 1.10675 * 10^{-10}\mathrm{F}$$

where the dielectric permittivity of vacuum, $\epsilon_O = 8.854 \cdot 10^{-12}\ \mathrm{F \cdot m^{-1}}$. The filled cells were placed in a Linkam THMS 600 heating stage equipped with a TMS 91 control unit (± 0.1 K) for temperature control. The UV response of the compounds was studied using a UV light source, the Dymax BlueWave® QX4TM LED Spot-Curing System, with a focus lens of 8 mm in diameter. In selected experiments, the UV light intensity was varied and measured using a Dymax ACCU-CALTM 50-LED with a UV light detector, located at the same distance from the light source as the Linkam THMS 600 sample holder. Geometry optimisations of the azobenzene dimers in the *trans* and *cis* conformations were performed using density functional theory (DFT) calculations at the B3LYP-6-31G(d) level of theory, with the Gaussian09 software.[29] Visualisation of the calculated dipoles and electrostatic isosurfaces were generated using Gaussview 5,[30] and space-filling models were created from the optimised geometries using the QuteMol package.[31] Further details of the experimental conditions used to measure the dielectric response are given in the results section.

3. Results and discussion

Phase behaviour. The three dimers, CB6OAzO2, CB6OAzO6 and CB6OAz6, display enantiotropic liquid crystal behaviour, assessed by polarised optical microscopy, POM. Observations were made using quartz and Instec cells, confirming the planar alignment of the director in the latter. The nematic phases were assigned based on the observation of Schlieren textures, with two- and four-brush singularities, see **Fig. 4**. On cooling, N_{TB} phases formed, assigned by the appearance of parabolic defects and striped textures,[32] accompanied by the cessation of optical flickering related to director fluctuations in the conventional nematic phases.[33]

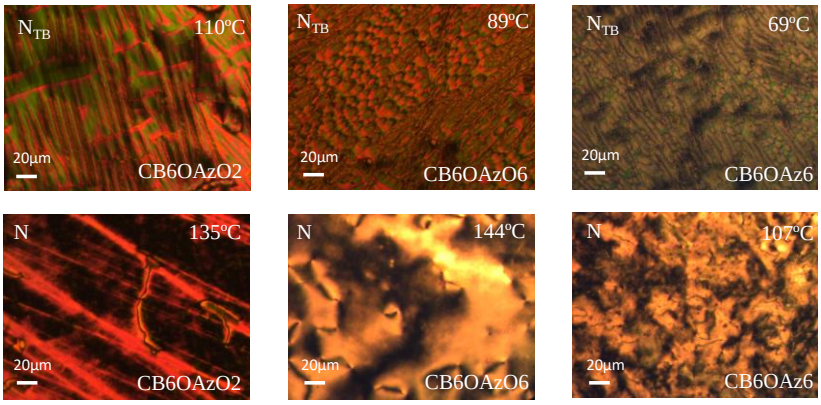

Figure 4. Optical textures of the dimers obtained by polarised optical microscopy, POM, in the twist-bend nematic phase (N_{TB}) and the conventional nematic phase (N). Temperatures are indicated on the micrographs.

Table 1 summarises the thermal parameters of the dimers obtained by DSC, see **Fig. 5** (and **Fig. ESI10** and **ESI11**). The table also contains the transitional properties for CB6OAzO4 for comparison purposes.[32] Increasing the terminal chain length in the CB6OAzO*n* series depresses both the nematic to isotropic, T_{NI}, and twist-bend nematic to nematic, T_{NTBN}, transition temperatures. This may be attributed to the dilution of the anisotropic interactions between the mesogenic units on increasing *n*. [34, 35] The melting point shows a more irregular dependence on *n.*

Table 1. Thermal parameters obtained by differential scanning calorimetry, DSC, and polarised optical microscopy, POM. Cr = crystal; N_{TB} = twist-bend nematic; N = nematic; I = isotropic.

Dimer	**DSC** **T/°C [ΔH(kJ mol^{-1})]**[a]
CB6OAzO2	Cr 136.3 [31.7] (N_{TB} 113.2 [-])[c] N 168.0 [1.14] I
CB6OAzO4[d]	Cr 104.8 [49.4] N_{TB} 105.5 [0.1] N 152.7 [1.4] I
CB6OAzO6	Cr 123.6 [27.0] (N_{TB} 97.6 [-])[c] N 143.0 [0.7] I
CB6OAz6	Cr 84.7 [43.4][b] (N_{TB} 79.1 [-])[c] N 118.4 [0.7] I

[a] Obtained from the second heating scan (rate = 10°C min^{-1}).
[b] Combined enthalpy of two Cr to Cr transitions.
[c] Obtained on cooling, very weak first-order transition.
[d] Taken from reference.[23]

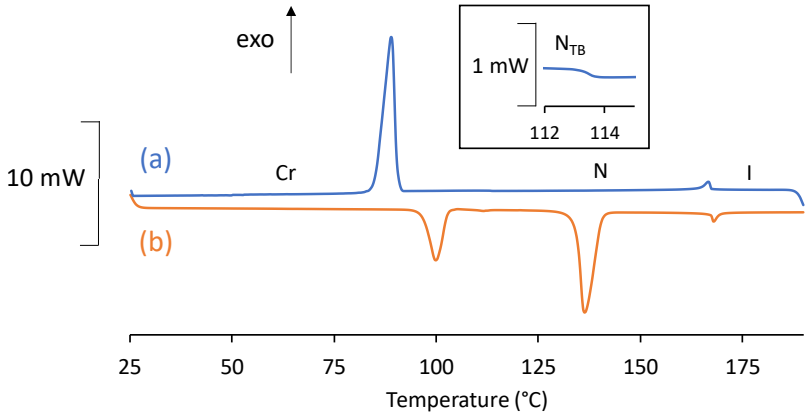

Figure 5. Differential scanning calorimetry, DSC, traces, for CB6OAzO2, obtained during the cooling scan (a) and second heating scan (b). Inset is magnified to reveal the N to N_{TB} transition.

CB6OAz6 shows the lowest transition temperatures of the dimers, see **Table 1**, and this may be attributed to the relative disposition of the terminal chain with respect to the azobenzene-based unit. Specifically, an alkoxy chain lies in the same plane to the ring to which it is attached whereas an alkyl chain protrudes at an angle. In addition, the absence of the ether group linking the terminal chain reduces dipolar interactions as well as packing efficiency, and we will return to this observation later. Experimentally, CB6OAz6 has the most accessible N_{TB} phase, as it shows the least tendency to crystallise.

Dielectric response. Fig. 6 illustrates the dielectric response, in terms of the dielectric loss factor, ε'', of CB6OAz6. The values were obtained between ITO slides treated for planar alignment, in the 10^7 – 10^3 Hz range, in isothermal steps on cooling from the isotropic phase. We used harmonic probe fields (1 V_{rms}) well below the threshold voltage of the Fréedericksz transition, and in the absence, V_{bias} = 0V, **Fig. 6(a)**, and the presence, V_{bias} = 35V, **Fig. 6(b)**, of a *bias* electrical field. The application of strong alternating electrical fields leads to similar profiles of ε^* as in **Fig. 6(b)** (19 V_{rms}, see **Fig. ESI12**). All the dimers exhibit higher dielectric permittivity values ($\varepsilon^* = \varepsilon' - i\,\varepsilon''$) than CB7CB, and this result is somehow expected due to the occurrence of dipole cancellation in symmetric dimers, such as, the CB*n*CB series. [36] We note, however, that the permittivity values that we have measured for our nonsymmetric CB6OAz(O)*n*s are still in the same range as those obtained for CB7CB or CB9CB. To some extent, the high dielectric values in symmetric dimers can be explained by the presence of hairpin conformers at sufficiently high temperatures, which avoids cancellation of the dipole moments between cyanobiphenyl groups.[37, 38]

The dimers display two main dielectric relaxations in the N and N_{TB} phases. At low frequencies, the so-called μ_1 mode is associated with flip-flop motions of the dipolar units in the dimers. The μ_1 mode is visible throughout the temperature range under study, and has weak intensity in the absence of strong bias (or V_{rms}) electric fields. The low amplitude of $\mu_{1,\perp}$ in **Fig. 6(a)** confirms the planar orientation of the nematic director in the ITO cells, and the polar cyanobiphenyl groups lie on average perpendicularly to the alternating electric field. Under the application of strong electrical fields (both DC and AC), the director re-aligns and adopts homeotropic configurations. The resulting dipolar response considerably increases, $\mu_{1,\parallel}$, with the dipoles of the CN groups now being parallel to the electric field, see **Fig. 6(b)** and **Fig. ESI12**. This behaviour is in excellent agreement with that of other liquid crystal dimers with positive dielectric anisotropy.[38]

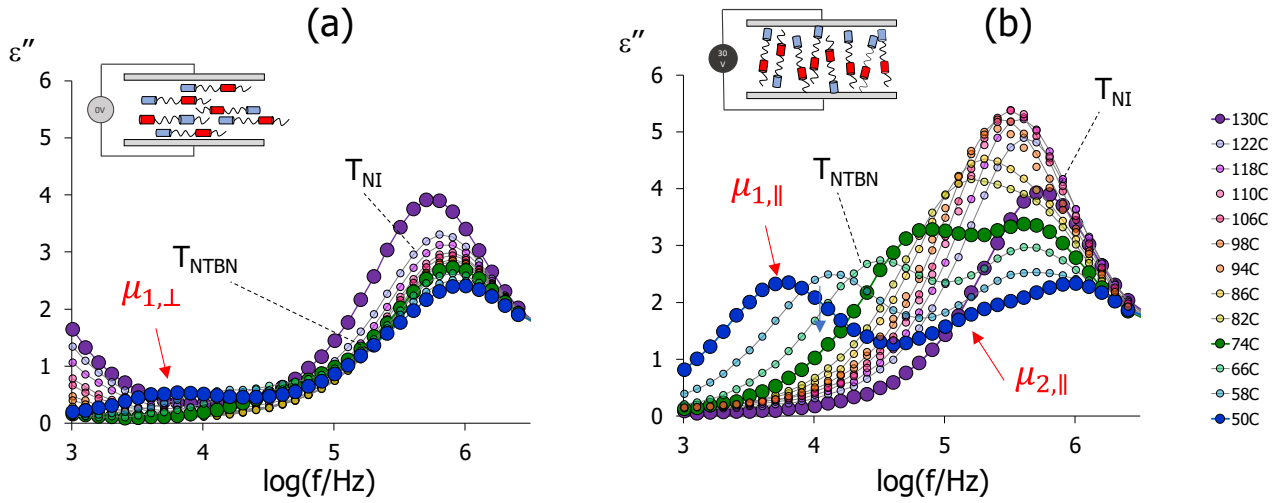

Figure 6. Dielectric loss factor, ε'', measured for CB6OAz6 in a planar cell on cooling from the isotropic phase (T = 130 °C) to the twist-bend nematic phase (T = 50 °C). Results obtained: (a) in the absence of an electrical field (V_{bias} = 0 V); (b) in the presence of a strong electric field (V_{bias} = 35 V). T_{NTBN} = 79.1 °C, T_{NI} = 118.4 °C.

At higher frequencies, a second relaxation mode, $\mu_{2,\parallel}$, is visible in homeotropically aligned samples, **Fig. 6(b)**. This has been associated with precessional motions of the dipoles around the director,[36] and merges with μ_1 at temperatures near T_{NI}. Unfortunately, this second contribution is obscured by a strong signal between 10^5 and 10^6 Hz, which is normally present when ITO electrodes are used in high frequency measurements.[39, 40] In order to characterise this mode, further experiments would be needed, using untreated metal electrodes.

We have calculated the dipole moment of the optimised geometries for the *trans* isomers of two representative dimers (CB6OAzO2 and CB6OAz6) using quantum mechanical density functional theory (DFT). The lowest energy state of compounds with ether-linked spacers has been found to include a gauche linkage,[41] but the energy difference between this conformation and the all-*trans* state is sufficiently small (*ca* 1 kJ mol^{-1}) that it is expected the greater linearity of the all-*trans* state will be more favourable within a liquid crystalline environment.[42] Thus, the geometry optimisations were carried out with the central spacer in the all-*trans* conformation, and this assumption is in accord with similar recent studies.[43] Dipole moment values of $\vec{\mu}$ = 4.2021 D, for *trans*-CB6OAzO2, and $\vec{\mu}$ = 4.1126 D, for *trans*-CB6OAz6, were obtained, see **Fig. 7(a)** and **Fig. 7(b)**, respectively. These similar values are mainly attributed to the highly polar cyanobiphenyl groups for which $\vec{\mu} \sim 6.5\ D$,[44] whereas the contribution of the *trans*-azobenzene groups to the dielectric response of the dimers must be weaker, due to their lower dipole moments, $\vec{\mu} \sim 0.1\ D$.[45-47] As a matter of fact, analogous calculations for the so-called CB7CB (symmetric) and CB6OCB (nonsymmetric) dimers, gave higher dipole moments than our materials (6.4378 D and 4.6135 D, respectively), highlighting the contribution of the second cyanobiphenyl unit to the dielectric strength, see **Fig. ESI13**.

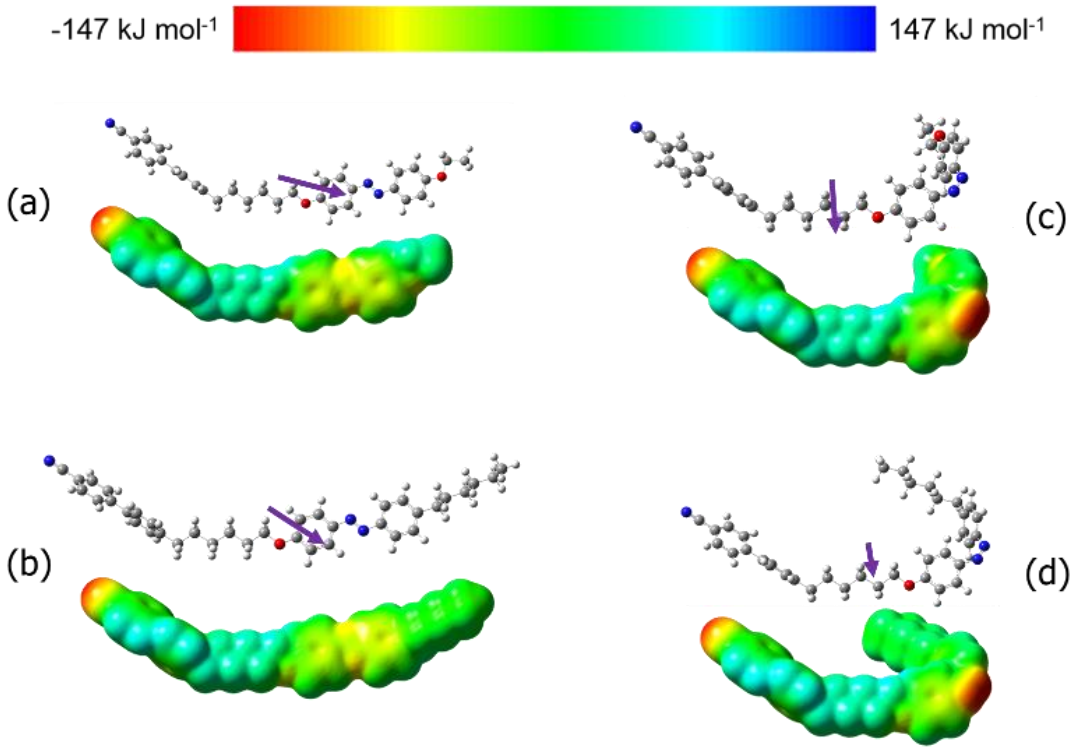

Figure 7. Ball-and-stick models (top) and electrostatic potential surfaces (lower) of: (a) *trans*-CB6OAzO2; (b) *trans*-CB6OAz6; (c) *cis*-CB6OAzO2; (d) *cis*-CB6OAz6, isomers, corresponding to their optimised molecular geometries obtained by DFT. Arrows indicate the direction of their molecular dipoles.

The realignment of the director required to yield homeotropic alignment must be led by reorientation of the dipole moments in **Fig. 7**, under sufficiently strong electric fields. We have determined the Fréedericksz transitions, V_{th}, by applying increasing alternating fields, in the range 0 to 19 V_{rms}, see **Fig. 8(a)** and **Fig. ESI14.**[48, 49] The real component of the complex capacitance, C', and also the dielectric elastic constant, ε', of the dimers, were calculated at a fixed frequency of 5 kHz, in order to avoid undesired ionic effects at low temperatures. The Fréedericksz transitions fall between V_{th} = 0.5 – 3 V, in agreement with those of liquid crystal dimers reported elsewhere.[37] Based on these C' *vs* V_{rms} curves, we have estimated the splay, K_1, and bend, K_3, elastic constants in the nematic phase, and the results for CB6OAzO2 are shown in **Fig. 8(b)** and **Fig. 8(c)**, respectively (see details in supplementary information).

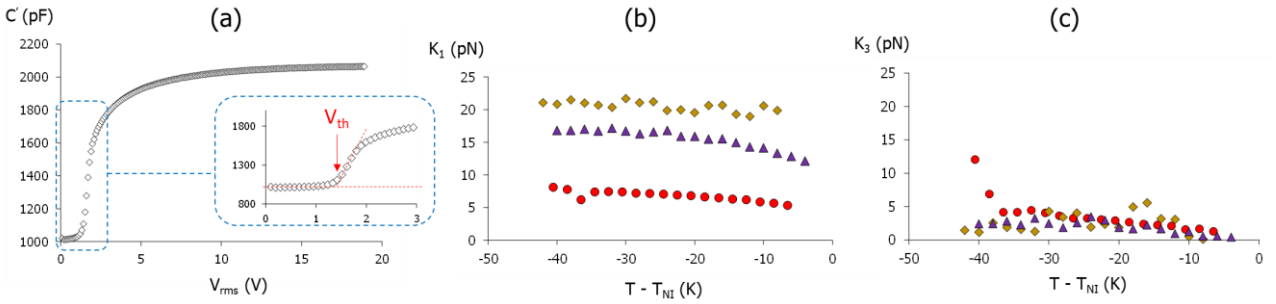

Figure 8. (a) Capacitance, C', as a function of the voltage (V_{rms}) for CB6OAzO2, obtained in the nematic phase (T = 146 ºC), and estimation of Fréedericksz transition, V_{th}. Estimation of the (b) splay elastic (K_1), and (c) bend elastic (K_3) constants of the three dimers in their nematic phases, on cooling from their nematic to isotropic transitions, T_{NI}: (▲) CB6OAzO6; (◆) CB6OAzO2; (●) CB6OAz6.

The three dimers show values of the elastic constant at the high-end but in the same range (10^{-12} N) as other liquid crystal dimers, obtained using comparable, but not identical, methods.[37, 50] As expected, the splay elastic constant is higher than the bend elastic constant, $K_1 > K_3$. The low values of K_3 reflect the tendency of the dimers to adopt curved geometries, and ultimately exhibit N_{TB} behaviour. K_1 increases according to CB6OAzO2 > CB6OAzO6 > CB6OAz6, whereas the bend elastic constant, K_3, does not follow a clear trend. These results are in good agreement with the trend observed in T_{NTBN} seen in **Table 1**. The splay elastic constant tends to show a weak increase on cooling through the nematic phase, which indicates a tendency to adopt bent geometries.[51] From our data, however, it is difficult to draw conclusions concerning the behaviour of the bend elastic constant. K_3 is predicted to decrease on approaching T_{NTBN}.[2] In contrast, our K_3 values appear to increase on cooling, and this trend is particularly evident for CB6OAz6, which exhibits the highest K_3 values of these materials at low temperatures. The scattering of the results may be attributed, at least in part, to the presence of local structure fluctuations when approaching the N - N_{TB} transition, due to the progressive formation of helices existing in a relatively broad range of temperatures.[52]

Another factor that may explain the moderately high K_1 and K_3 values seen here may be the strong dielectric anisotropy, $\Delta\boldsymbol{\varepsilon}$, of these dimers, also consistent with their high $\vec{\mu}$ values calculated by DFT. In **Fig. 9** we plot the different components of the static dielectric permittivity (5 kHz) of CB6OAz6, ε', obtained on cooling from the isotropic phase (see also **Fig. ESI15**). $\Delta\varepsilon$ is zero in the isotropic phase, and starts increasing on cooling in the vicinity of the nematic to isotropic transition, T_{NI}=118.4ºC. On further cooling, this effect is offset by the increase of the nematic order parameter, resulting in a higher population of dimers with more extended conformations that promote net-zero dipole distributions.[53] We also note that the dimers show only small deviations between the parallel components of the static permittivity, $\varepsilon_{\parallel}$, measured using AC or DC fields.

Our results are comparable to those obtained for odd-membered cyanobiphenyl dimers, CBnCBs, but with some differences.[3, 37, 38, 54] The higher $\varepsilon_{\parallel}$ and $\Delta\varepsilon$ values in **Fig. 9**, may be explained by the nonsymmetry of the dimers, which results in non-cancellation of the dipole moments of the cyanobiphenyl groups that occurs in the CB*n*CB dimers, but could also, in part, result from favourable mixed core-interactions that are entropically favoured. The strong electrical fields (35 V and 19 V_{rms}) applied to align the director above V_{th} may promote excitation of the azobenzene cores in the dimers from their highest occupied to their lowest unoccupied molecular orbital energy levels (HOMO and LUMO, respectively, see **Fig. ESI16**). The strong delocalisation of charge distributions in their excited LUMO states could facilitate electrostatic interactions between neighbouring dimers,[55] which is consistent with the appreciable values of current exhibited under these conditions (~10^{-3} A and ~10^{-4} A, respectively). The $\boldsymbol{\varepsilon}_{\perp}$ values of the nonsymmetric dimers, on the other hand, undergo a smooth decrease when approaching T_{NTBN} in the nematic phase ($T > T_{NTBN}$), and increase when entering the twist-bend nematic phase ($T < T_{NTBN}$), see **Fig. 9(a)**, whereas for CB7CB and CB9CB, $\boldsymbol{\varepsilon}_{\perp}$ decreases on cooling in both the N and N_{TB} phases, **Fig. ESI17.**[3, 37] This suggests that the azobenzene fragments in our dimers promote a positive dielectric contribution perpendicular to the slides, due to the persistence of non-cancelled molecular dipoles.

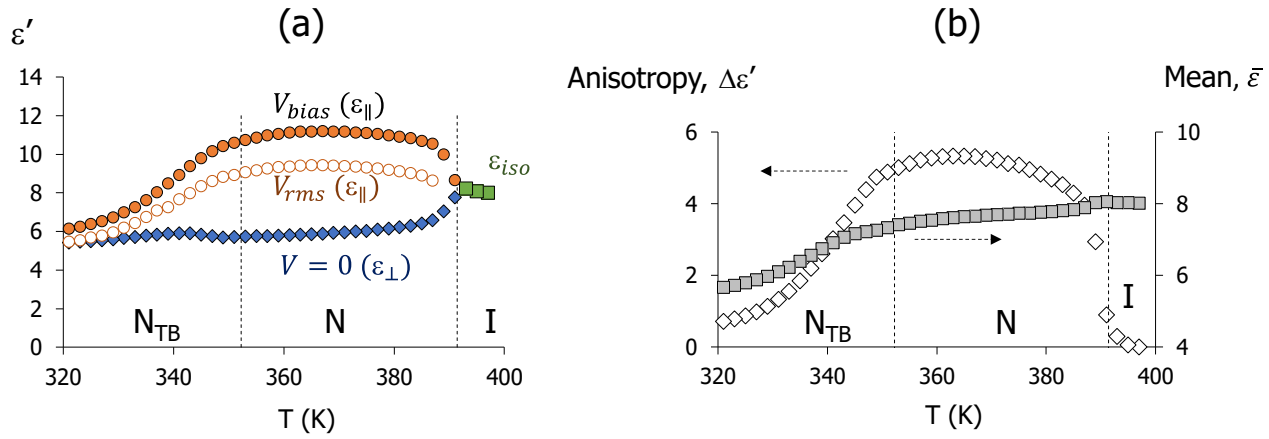

Figure 9. (a) Components of the dielectric elastic constant, ε', measured for CB6OAz6, in isothermal steps on cooling from the isotropic phase, I (ε_{iso}), through the nematic phase, N, to the twist-bend nematic phase, N_{TB}: perpendicular V = 0 ($\boldsymbol{\varepsilon}_{\perp}$) and parallel with V_{bias} = 35 V and V_{rms} = ± 19 V ($\varepsilon_{\parallel}$). (b) Dielectric anisotropy, $\Delta\varepsilon = \varepsilon_{\parallel}(V_{bias}) - \varepsilon_{\perp}$, and mean dielectric permittivity, $\bar{\varepsilon} = (\varepsilon_{\parallel} + 2\varepsilon_{\perp})/3$. Vertical dotted lines show T_{NI} = 118.4 °C and T_{NTBN} = 79.1 °C.

Light-response and phase control. As expected, the presence of azobenzene groups endows these dimers with light responsive character. More specifically, their UV-vis spectra show an intense band centred at ~350 nm, corresponding to the π–π* transition of the azobenzene *trans* conformer, together with a much weaker absorption band at ~450 nm, associated with the

symmetric forbidden n–π* transition,[56] see **Fig. ESI18**. Irradiation with actinic light at 365 nm results in a fast *trans*-to-*cis* photoisomerisation, with a dramatic decrease in intensity of the π–π* transition and a simultaneous, though less marked, increase of the n–π* transition band.

On irradiating the dimers with 365 nm light in the twist-bend nematic phase, they undergo reversible and isothermal phase transitions, N_{TB} - N - I, that can be monitored using POM. This behaviour has been attributed to the reduction in shape anisotropy caused by the presence of the less linear *cis* group after photoisomerisation.[23] These phase transitions occur in a few seconds, and the kinetics are highly sensitive to the irradiation dose applied, see **Fig. ESI19**. The shorter terminal chains of CB6OAzO2 promote faster relaxations, and by comparison CB6OAz6 requires considerably longer times to relax back into the N_{TB} phase. Indeed, for CB6OAz6 we could not observe this relaxation in some experiments at temperatures below $T\text{-}T_{NTBN}$ = -10 K.

In order to study these photolytically-driven transitions and their kinetics, we have monitored the static permittivity of the dimers as a function of UV irradiation, temperature and time. More specifically, we have measured ε' in planar aligned samples, using ITO cells connected to the Solartron 1620 impedance analyser, at a fixed frequency of 5 KHz. Above the ITO cell, we placed the UV Dymax lamp at a fixed distance, and we varied the UV dose densities. In additional experiments, we have performed simultaneous POM observations, to directly monitor phase behaviour and correlate those with the dielectric results. We note that our measurements and observations are reproducible after several irradiation cycles, precluding the possibility of thermal degradation effects on our samples.

Firstly, we show in **Fig. 10** phase diagrams of the samples as a function of UV light dosage, obtained on cooling from their isotropic phases at 2 ^{o}C min^{-1}, based on the dependence of ε' reported in **Fig. 9**, and **Fig. ESI20** illustrates some examples. The results are reproducible on heating scans at the same rate.

Upon light exposure, both the nematic to isotropic, T_{NI}, and the twist-bend nematic to nematic, T_{NTBN}, transition temperatures of the three dimers drop, due to the reduction of order after *trans*-to-*cis* isomerisation, and these values further decrease on increasing the intensity.[57] We note, however, that whereas T_{NTBN} undergoes large decreases that can reach $-\Delta T(T_{NTBN}) \sim 30^{o}$C even at low UV dosages, T_{NI}, on the other hand, decreases by just a few degrees even upon very strong irradiation doses (up to 1000 mW·cm^{-2} for CB6OAzO2). This different behaviour may be attributed, in part, to the stronger dependence on molecular shape of the thermodynamically weak N_{TB} to N transition, but also to the temperatures at which both transitions take place. The *cis*-to-*trans* thermal back-isomerisation must be favoured at higher temperatures, hence in photostationary states occurring around T_{NI} we should expect larger amounts of *trans* isomers than at the lower T_{NTBN} temperatures. We suggest that the small concentration of *cis* isomers near T_{NI} may not be

sufficient to destabilise the N phase over a broad range of temperatures and UV dosages. Indeed, for CB6OAzO2 we have observed that the N phase remains stable under prolonged irradiation (1000 mW cm^{-2}) at isothermal conditions of T- T_{NI} = - 8 K.

CB6OAz6 shows much lower transition temperatures and, as a consequence, a larger concentration of *cis* isomers is expected in its photostationary state compared to the CB6OAzO*n* dimers, resulting in larger depressions of T_{NI} and T_{NTBN}. The N_{TB} phase of CB6OAz6 is extinguished in **Fig. 10(c)** at much lower UV irradiation doses than those of CB6OAzO6 and CB6OAzO2 (**Fig. 10(a)** and **Fig. 10(b)**, respectively). UV irradiation also promotes the appearance of re-entrant nematic (N_{re}) and isotropic (I_{re}) phases on cooling (≥ 20 mW·cm^{-2}), coexisting in biphasic regions under some conditions of irradiation and temperature, and which are stabilised at increasing dosage values, due to a shift of the photostationary equilibrium state towards higher concentrations of *cis* isomers. These re-entrant phases form from nematic phases (see **Fig. ESI21**), supported by the observation of dark fields that do not revert under the application of mechanical pressure between untreated glasses. At sufficiently high irradiation dosages the three dimers show no liquid crystalline behaviour.

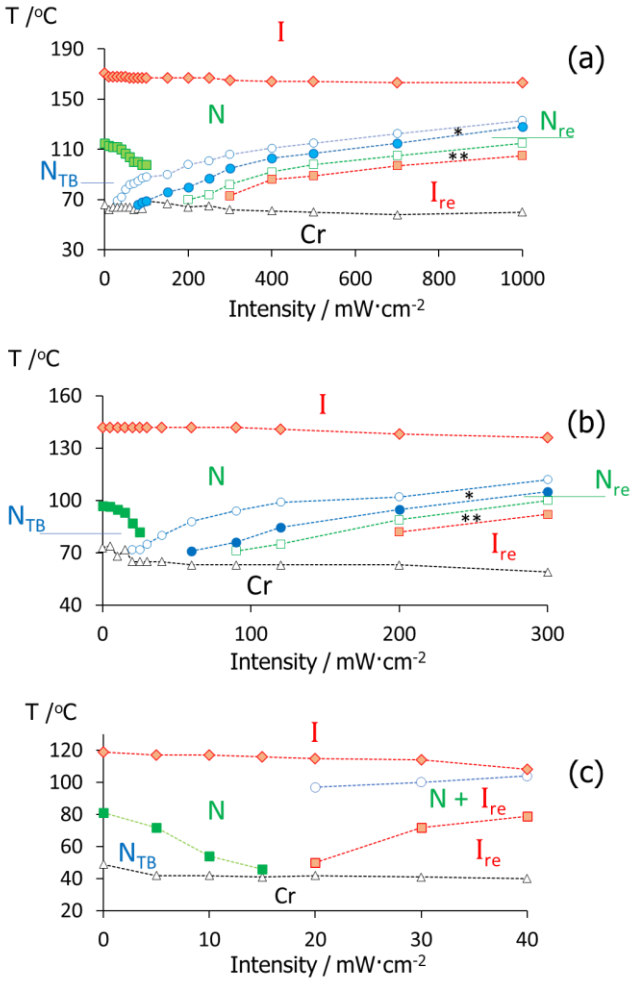

Figure 10. Phase diagrams obtained in planar cells by measuring ε' (5 kHz) upon cooling the dimers (2 $^{o}C \cdot min^{-1}$) during irradiation with different dosages of UV light, indicating the transitions between isotropic (I), nematic (N), twist-bend nematic (N_{TB}) phases, re-entrant isotropic (I_{re}) and nematic (N_{re}) phases, and biphasic regions: N + N_{re} (∗), N_{re} + I_{re} (∗∗) and N + I_{re}: (a) CB6OAzO2; (b) CB6OAzO6; (c) CB6OAz6. Empty squares and circles correspond to the beginning of the biphasic range observed on cooling.

The phase diagrams in **Fig. 10** have been obtained under dynamic conditions, and it is also interesting to study the isothermal response of the dimers. The behaviour of CB6OAzO2 on illumination in the twist-bend nematic phase (95^{o}C, T-T_{NTBN} ~ - 18.2 K), is shown in **Fig. 11(a)**, which displays the dependence of ε' after irradiation with a low intensity dosage (150 mW cm^{-2}). After UV exposure (UV_{on}), ε' decreases, and the sample undergoes the N_{TB} to N transition. On continued irradiation in the nematic phase, the ε' values plateaus, and no further transition is observed after one minute. When the UV light is switched off (UV_{off}), ε' decreases slightly before increasing and reaching a steady state when the N to N_{TB} transition takes place, and recovers its initial value. **Fig. 11(b)** was obtained at the same temperature (T-T_{NTBN} = - 18.2 K), but using a larger UV dose (1000 mW cm^{-2}). After a similar initial drop, coinciding with an extremely fast N_{TB} - N transition, the ε' values increase sharply going through the N_{re} phase and finally reaching a plateau at higher values than seen in **Fig. 11(a)**, in the I_{re} phase. This behaviour is reversible, including I_{re} - N_{re} - N_{TB} transitions on switching the UV off. The dielectric time-response to UV light shown in **Fig. 11** is consistent with previous opto-dielectric effects reported by other authors on, for example, mixtures of azobenzene guests and liquid crystalline hosts.[28, 58] These results are also consistent with the phase behaviour seen in **Fig. 10**, **Fig. ESI20** and **Fig. ESI21**.

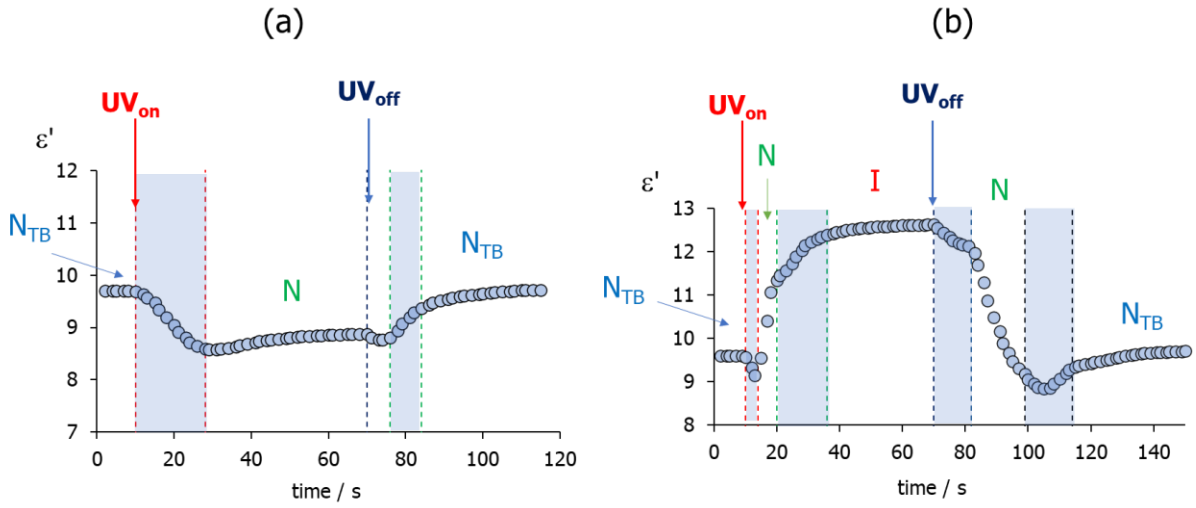

Figure 11. Isothermal UV response of CB6OAzO2 in the twist-bend nematic phase (N_{TB}, T-T_{NTBN} = - 18.2 K), measured in a planar cell, ε' ($\varepsilon_{\perp}$) *vs* time, applying different UV intensities:(a) 150 mW cm^{-2}; (b) 1000 mW cm^{-2}. Dotted lines indicate total disappearance (T_{NI}) or partial appearance (T_{IN})

of birefringent regions under the polarised microscope, associated with the nematic (N) to isotropic (I) transition. Shaded regions indicate coexistence of two phases.

The initial drop in ε', see **Fig. 11(a)**, reflects a fast *trans*-to-*cis* photoisomerisation, which for the analogous nonsymmetric dimer CB6OAzO4 takes place in a few seconds at the N_{TB} phase,[23] and which is also in agreement with **Fig. ESI18**. This reduction in ε' may have a two-fold explanation. On one hand, dimers in the *cis* form have smaller dipole moments, as calculated by DFT ($\vec{\mu}$ = 3.7090 D, for CB6OAzO2, and $\vec{\mu}$ = 2.4108 D, for CB6OAz6), compared to their respective *trans* counterparts, see **Fig. 7(c)** and **Fig. 7(d)**. On the other hand, the formation of the *cis* isomers disrupts the N_{TB} helicoidal order to promote the N_{TB} - N transition, and the director of the nematic phase may lie parallel to the electrode surfaces, and hence the dipole moment aligns perpendicular to the electrical field. We note, however, that the resulting dipole moment of the *cis*-CB6OAzO2 isomers is perpendicular to the molecular axis, see **Fig. 7(c)**, and this may explain the subsequent slight increase observed for ε' in **Fig, 11(a)**. After a certain time, the values of ε' plateaus, reflecting a mixed population of *cis* and *trans* isomers in equilibrium.

Under the experimental conditions in **Fig. 11(a)** (150 mW·cm^{-2}, T=95^{o}C), the population of *trans* isomers may be sufficiently high to sustain the N phase of CB6OAzO2, which is depressed by a few degrees, see **Fig. 10(a)**. At higher UV doses, **Fig. 11(b)**, the larger concentration of *cis* isomers with their nonuniform bent geometries weakens the interactions between the *trans* isomers to a greater extent, and neither the N_{TB} and N phases are stable. The sample goes through a fast N_{TB} - N transition, followed by a biphasic region in which nematic and isotropic phases coexist, and becomes completely isotropic. This destroys the initial planar alignment, which explains the increase in the ε' values until reaching a plateau value in the isotropic phase,[59] but may also be explained by the formation of N_{re} (and I_{re}) phases observed in **Fig 10(a)**, resulting in larger ε' values than those of the N phase achieved in the dark, **Fig. ESI20**. The slightly greater recovery times after UV_{off}, compared to the response after UV_{on}, were expected, due to the slower thermal back relaxation. We also note that the ε' values comprise contributions from a mixed population of *cis* and *trans* isomers in equilibrium (under UV-illumination), with dipole moments having different relative directions with respect to their respective long molecular axes. Slight discrepancies between the static and dynamic results may again reflect the role of kinetics on the phase behaviour of these dimers.

Even though the three dimers show comparable UV responses, in terms of their ε' *vs* time curves, CB6OAzO2 and CB6OAzO6 display similar times required to achieve their plateau values (t ~ 35 s), whereas CB6OAz6 has a much slower response (t ~ 60 s). We have further studied the effect of the UV dosage on the kinetics of the CB6OAz6 phase transitions, and **Fig. 12(a)** illustrates the

isothermal N_{TB} - N - I transitions of this dimer at 65ºC ($T-T_{NTBN}$ = - 15 K), and **Fig. 12(b)** the isothermal N - I transition at 100ºC ($T-T_{NI}$ = - 17 K). These results are consistent with **Fig. 10(c)**, since all the intensities applied fall above the threshold values for which nematic and twist-bend nematic phases are destroyed upon UV irradiation (> 40 mW·cm^{-2}). As expected, on increasing light intensity, the transitions occur faster, see **Fig. 12**. This may be explained again by the larger concentrations of *cis* isomers. Upon irradiation with sufficiently high UV dosages in the N_{TB} phase (> 190 mW·cm^{-2}, $T-T_{NTBN}$ = - 15 K), we observe incomplete I - N and N - N_{TB} relaxations for at least 15 minutes after irradiation ceases (UV_{off}). Instead, we see the coexistence of isotropic, nematic and twist-bend nematic phases under the microscope, and this incomplete back relaxation can be monitored by the lack of recovery of the initial ε' values in **Fig. 12(a)**. These results may reflect slow CB6OAz6 molecular rearrangements to reform the helices in the N_{TB} phase, at least at such low temperatures, attributed to the presence of the hexyl terminal chain that disrupts local order.[60] The UV-driven nematic to isotropic transition of CB6OAz6, on the other hand, is fully reversible, as seen in **Fig. 12(b)** ($T-T_{NI}$ = - 17 K), probably assisted by the greater thermal energy available at higher temperatures.

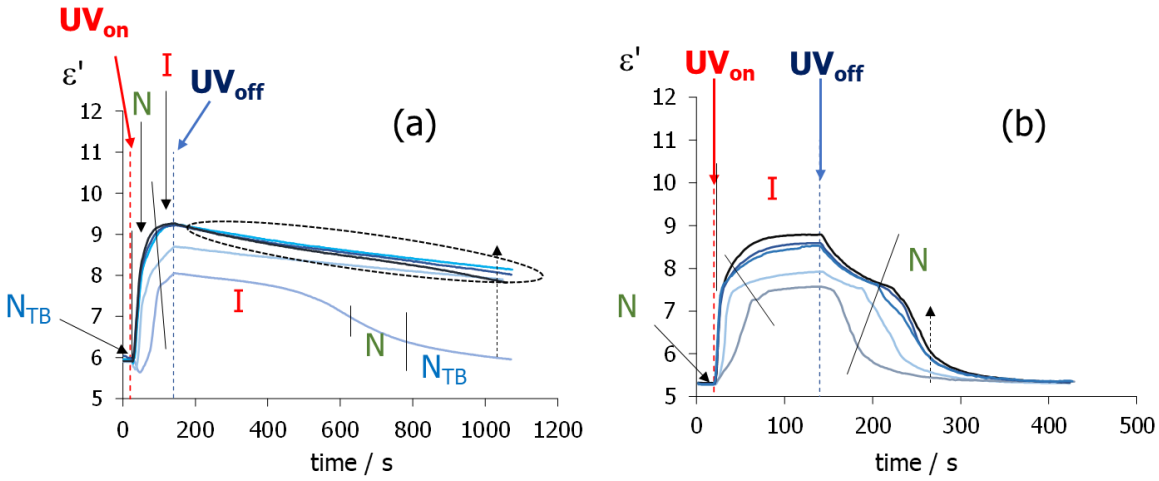

Figure 12. Time dependence of the static dielectric permittivity, ε', measured under planar alignment conditions (5 KHz, V_{bias}=0V) of CB6OAz6, upon application of UV light (UV_{on}) and relaxation (UV_{off}), at (a) T=65ºC (N_{TB} phase) and (b) T= 100ºC (N phase). Solid lines indicate start or end of phase transitions; dotted arrows indicate increasing UV intensity (80, 190, 430, 610 and 810 mW·cm^{-2}). Dotted ellipse indicates an unresolved region of I, N and N_{TB} coexistence.

The dynamic effects observed in **Fig. 12(a)** for the dielectric response and phase behaviour under UV irradiation of CB6OAz6 are reproducible in different cycles, as illustrated in **Fig. 13(a)** (ε' measured in the N_{TB} phase) and **Fig. 13(b)** (ε' measured in the N phase). Whereas the N - I relaxation is fully reversible, the I - N and N - N_{TB} relaxations are not on the time scale investigated.

The temperature dependence of this effect was studied in further measurements of the static dielectric permittivity (5 kHz) taken in planar cells for CB6OAz6, and in the absence and the presence of bias electrical fields, following UV-irradiation cycles of 120 mW·cm^{-2}, see **Fig. ESI22**. As expected, we found that $\varepsilon_{\perp}$ and $\varepsilon_{\parallel}$, become equal under UV irradiation due to a loss of alignment by the presence of *cis* isomers, in agreement with **Fig. 10** to **Fig. 12**. As we approach the T_{NTBN} transition in the nematic phase, and also through the twist-bend nematic phase, the original dielectric values do not recover when the UV irradiation ceases. This behaviour is not observed in similar experiments for CB6OAzO2 and CB6OAzO6, which show reversible and fast N_{TB} - N - I transitions across the temperature range under study. This observation confirms the role of the terminal alkyl chain on the molecular dynamics of CB6OAz6, by delaying or hindering, at least partially, the molecular rearrangements necessary to undergo helicoidal arrangements in the N_{TB} phase.

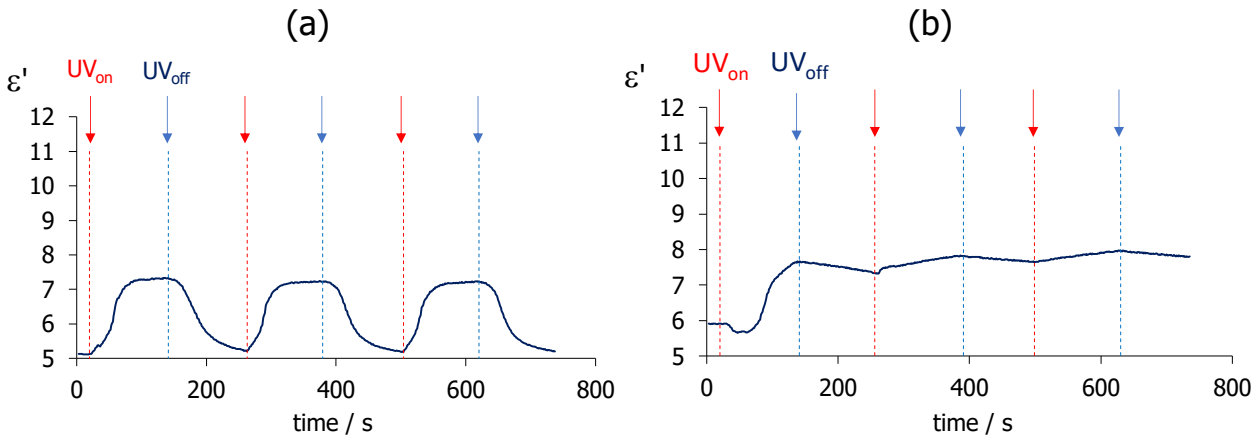

Figure 13. Time dependence of the static dielectric permittivity, ε', measured under planar alignment conditions for CB6OAz6 (5 KHz, V_{bias}=0V), during the application of UV-irradiation cycles (120 mW·cm^{-2}): (a) in the nematic phase (T=100ºC); (b) in the twist-bend nematic phase (T=65ºC).

4. Conclusions

The three nonsymmetric dimers studied show conventional nematic and twist-bend nematic behaviour, sustained by the molecular curvature endowed by the -$(CH_2)_6$O- odd-membered spacer. CB6OAzO2 and CB6OAzO6 display higher twist-bend nematic to nematic transition temperatures than CB6OAz6, which are consistent with their smaller values of the bend elastic constant, K_3, presumably due to the alkoxy terminal chains that enhance the spatially uniform curvature.[61, 62]

The three dimers show a strong dielectric response and anisotropy under alternating and bias electrical fields, and this may be promoted by their nonsymmetry, which prevents the strong dipole moment of the cyanobiphenyl fragments from cancelling. Interestingly, the dielectric elastic constants of the three dimers measured under conditions of planar alignment, $\varepsilon_{\perp}$, increase when entering the twist-bend nematic phase on cooling from the nematic phase, opposite to what is reported for symmetric cyanobiphenyl dimers.[37] This is attributed to the presence of the azobenzene units, and may reflect the local arrangements of the cyanobiphenyl groups within the N_{TB} helices.

As expected, the three dimers are photo-sensitive, and UV exposure causes slight decreases in T_{NI}, and larger drops in T_{NTBN}, triggered by a disruption in molecular interactions and liquid crystal order by the *cis*-isomers.[23] Upon UV illumination with sufficiently high intensities, re-entrant nematic and isotropic phase appear at low temperatures, due to the larger concentrations of *cis* isomers of the dimers in the photostationary equilibria. Samples undergo isothermal N_{TB} - N - I transitions, which depend on UV irradiation dose and temperature, and the dynamics of these transitions have been qualitatively studied by monitoring the dielectric permittivity and textural response under the polarised microscope. The N_{TB} to N transition occurs very rapidly upon UV irradiation, and it is possible to stabilise the nematic phase at temperatures below T_{NTBN}, or to promote full isotropisation at higher UV doses or lower temperatures.

CB6OAz6 undergoes much slower isothermal transitions than the alkoxy-terminated dimers, and under some conditions of time and UV dosage, this dimer does not reverse back into the twist-bend nematic phase after irradiation ceases. We have attributed this effect to the disruption of the interactions by the terminal alkyl chain that hinders, at least to some extent, cooperative rearrangements necessary to form the N_{TB} structures. These findings open the exciting possibility to develop systems capable of "storing" part of the dielectric permittivity after complete On-Off-On cycles (operating in the N_{TB} range), and also act as a memory device driven by On – Off fully reversible processes (operating in the N range), and being controlled by UV exposure and intensity.

Our results provide a detailed and comprehensive description of the photochromic response of these new nonsymmetric dimers showing liquid crystallinity, and more precisely twist-bend nematic behaviour, in terms of molecular structure, temperature, time and UV irradiation energy. Their responsive character will be further investigated with the aim to develop new photonic materials, flexoelectric memory devices or energy harvesters,[63] and to tune the N_{TB} behaviour of new materials *via* composition and light stimuli, by, for example, controlling the pitch of the helicoidal arrangements upon illumination cycles.[26]

Conflicts of interest

There are no conflicts to declare.

Acknowledgements

AMF would like to acknowledge the Scottish Government and the Royal Society of Edinburgh, for the award of one SAPHIRE project, the Carnegie Trust for the Universities of Scotland, for the award of the RIG008586 project, the Royal Society, for the Research Grant RGS\R1\201397, and the Royal Society of Chemistry, for the award of the mobility grant M19-0000. AMF and AK would also like to acknowledge the Carnegie Trust for the Universities of Scotland, for the award of one Carnegie Trust Vacation Scholarships. All authors would like to thank the School of Engineering and the Department of Chemistry of the University of Aberdeen, for financial support.

References

1. Meyer R. R. Balian, G. Weil, editors. Molecular fluids. New York: Gordon and Breach; 1976. .

2. Dozov I. On the spontaneous symmetry breaking in the mesophases of achiral banana-shaped molecules. Europhys Lett 2001 OCT 2001;56(2):247-53.

3. Cestari M, Diez-Berart S, Dunmur DA, Ferrarini A, de la Fuente MR, Jackson DJB, Lopez DO, Luckhurst GR, Perez-Jubindo MA, Richardson RM, et al. Phase behavior and properties of the liquid-crystal dimer 1 ",7 "-bis(4-cyanobiphenyl-4 '- yl) heptane: A twist-bend nematic liquid crystal. Physical Review E 2011 Sep 16;84(3).

4. Walker R, Pociecha D, Storey JMD, Gorecka E, Imrie CT. The chiral twist-bend nematic phase (N*(TB)). Chemistry-a European Journal 2019 OCT 17;25(58):13329-35.

5. Henderson PA, Imrie CT. Methylene-linked liquid crystal dimers and the twist-bend nematic phase. Liquid Crystals 2011 2011;38(11-12):1407-14.

6. Jakli A, Lavrentovich OD, Selinger JV. Physics of liquid crystals of bent-shaped molecules. Reviews of Modern Physics 2018 NOV 20;90(4):045004.

7. Sreenilayam SP, Panov VP, Vij JK, Shanker G. The N-TB phase in an achiral asymmetrical bent-core liquid crystal terminated with symmetric alkyl chains. Liquid Crystals 2017;44(1):244-53.

8. Mandle RJ, Goodby JW. A liquid crystalline oligomer exhibiting nematic and twist-bend nematic mesophases. Chemphyschem 2016 APR 4;17(7):967-70.

9. Mandle RJ. Designing liquid-crystalline oligomers to exhibit twist-bend modulated nematic phases. Chemical Record 2018 SEP;18(9):1341-9.

10. Mandle RJ, Goodby JW. A novel nematic-like mesophase induced in dimers, trimers and tetramers doped with a high helical twisting power additive. Soft Matter 2018 NOV 21;14(43):8846-52.

11. Mandle RJ, Stevens MP, Goodby JW. Developments in liquid-crystalline dimers and oligomers. Liquid Crystals 2017;44(12-13):2046-59.

12. Tuchband MR, Paterson DA, Salamonczykc M, Norman VA, Scarbrough AN, Forsyth E, Garcia E, Wang C, Storey JMD, Walba DM, et al. Distinct differences in the nanoscale behaviors of the twist-bend liquid crystal phase of a flexible linear trimer and homologous dimer. Proc Natl Acad Sci U S A 2019 MAY 28;116(22):10698-704.

13. Stevenson WD, An J, Zeng X, Xue M, Zou H, Liu Y, Ungar G. Twist-bend nematic phase in biphenylethane-based copolyethers. Soft Matter 2018 APR 28;14(16):3003-11.

14. Abberley JP, Killah R, Walker R, Storey JMD, Imrie CT, Salamonczyk M, Zhu C, Gorecka E, Pociecha D. Heliconical smectic phases formed by achiral molecules. Nature Communications 2018 JAN 15;9:228.

15. Salamonczyk M, Vaupotic N, Pociecha D, Walker R, Storey JMD, Imrie CT, Wang C, Zhu C, Gorecka E. Multi-level chirality in liquid crystals formed by achiral molecules. Nature Communications 2019 APR 23;10:1922.

16. Joshi V, Paterson DA, Storey JMD, Imrie CT, Chien L. Augmenting bragg reflection with polymer-sustained conical helix. Scientific Reports 2019 APR 2;9:5468.

17. Joshi V, Paterson DA, Storey JMD, Imrie CT, Chien L. Tunable backflow in chiral nematic liquid crystals via twist-bend nematogens and surface-localised &ITin&IT-&ITsitu &ITpolymer protrusions. Liquid Crystals 2017;44(14-15):2327-36.

18. Panov VP, Balachandran R, Nagaraj M, Vij JK, Tamba MG, Kohlmeier A, Mehl GH. Microsecond linear optical response in the unusual nematic phase of achiral bimesogens. Appl Phys Lett 2011 DEC 26;99(26):261903.

19. Xiang J, Li Y, Li Q, Paterson DA, Storey JMD, Imrie CT, Lavrentovich OD. Electrically tunable selective reflection of light from ultraviolet to visible and infrared by heliconical cholesterics. Adv Mater 2015 MAY 20;27(19):3014-8.

20. Abberley JP, Storey JMD, Imrie CT. Structure-property relationships in azobenzene-based twist-bend nematogens. Liquid Crystals 2019 NOV 14;46(13-14):2102-14.

21. Aya S, Jakli A, Imrie CT, Buka A, Araoka F. High ON/OFF ratio photoswitchable viscoelasticity in an azo-based dimer with twist-bend nematic phase. Liquid Crystals Xxii 2018;10735:UNSP 107350Z.

22. Paterson DA, Walker R, Abberley JP, Forestier J, Harrison WTA, Storey JMD, Pociecha D, Gorecka E, Imrie CT. Azobenzene-based liquid crystal dimers and the twist-bend nematic phase. Liquid Crystals 2017;44(12-13):2060-78.

23. Paterson DA, Xiang J, Singh G, Walker R, Agra-Kooijman DM, Martinez-Felipe A, Gan M, Storey JMD, Kumar S, Lavrentovich OD, et al. Reversible isothermal twist-bend nematic-nematic phase transition driven by the photoisomerization of an azobenzene-based nonsymmetric liquid crystal dinner. J Am Chem Soc 2016 APR 27;138(16):5283-9.

24. Aya S, Salamon P, Paterson DA, Storey JMD, Imrie CT, Araoka F, Jakli A, Buka A. Fast-and-giant photorheological effect in a liquid crystal dimer. Advanced Materials Interfaces 2019 MAY;6(9):1802032.

25. Aya S, Salamon P, Paterson DA, Storey JMD, Imrie CT, Araoka F, Jakli A, Buka A. High-contrast and fast photorheological switching of a twist-bend nematic liquid crystal. Jove-Journal of Visualized Experiments 2019 OCT(152):e60433.

26. Feng C, Feng J, Saha R, Arakawa Y, Gleeson J, Sprunt S, Z, C, Jákl A. Manipulation of the nanoscale heliconical structure of a twist-bend nematic material with polarized light. Physical Review Research 2020(2):032004(R).

27. Arakawa Y, Komatsu K, Ishida Y, Tsuji H. Thioether-linked azobenzene-based liquid crystal dimers exhibiting the twist-bend nematic phase over a wide temperature range. 2021 04/09;48(5):641-52.

28. Prasad SK, Madhuri PL, Satapathy P, Yelamaggad CV. A soft-bent dimer composite exhibiting twist-bend nematic phase: Photo-driven effects and an optical memory device. Appl Phys Lett 2018 JUN 18;112(25):253701.

29. M. J. Frisch, G.W. Trucks, H.B. Schlegel, G.E. Scuseria, M.A. Robb, J.R. Cheeseman, G. Scalmani, V. Barone, B. Mennucci, G.A. Petersson, et al, inventors. Gaussian (revision D. 01) gaussian inc, wallingford, CT. US patent . 2009.

30. Semichem Inc. GaussView 5 [computer program]. 2009. .

31. Tarini M, Cignoni P, Montani C. Ambient occlusion and edge cueing to enhance real time molecular visualization. IEEE Trans Visual Comput Graphics 2006 SEP-OCT;12(5):1237-44.

32. Paterson DA, Gao M, Kim Y, Jamali A, Finley KL, Robles-Hernandez B, Diez-Berart S, Salud J, Rosario de la Fuente M, Timimi BA, et al. Understanding the twist-bend nematic phase: The characterisation of 1-(4-cyanobiphenyl-4 '-yloxy)-6-(4-cyanobiphenyl-4 '-yl)hexane (CB6OCB) and comparison with CB7CB. Soft Matter 2016;12(32):6827-40.

33. Mandle RJ, Davis EJ, Lobato SA, Vol C-A, Cowling SJ, Goodby JW. Synthesis and characterisation of an unsymmetrical, ether-linked, fluorinated bimesogen exhibiting a new polymorphism containing the N-TB or 'twist-bend' phase. Physical Chemistry Chemical Physics 2014 2014;16(15):6907-15.

34. Walker R, Pociecha D, Strachan GJ, Storey JMD, Gorecka E, Imrie CT. Molecular curvature, specific intermolecular interactions and the twist-bend nematic phase: The synthesis and characterisation of the 1-(4-cyanobiphenyl-4-yl)-6-(4-alkylanilinebenzylidene-4-oxy)hexanes (CB6O.m). Soft Matter 2019 APR 21;15(15):3188-97.

35. Paterson DA, Crawford CA, Pociecha D, Walker R, Storey JMD, Gorecka E, Imrie CT. The role of a terminal chain in promoting the twist-bend nematic phase: The synthesis and characterisation of the 1-(4-cyanobiphenyl-4 '-yl)-6-(4-alkyloxyanilinebenzylidene-4 '-oxy)hexanes. Liquid Crystals 2018 DEC 8;45(13-15):2341-51.

36. Lopez DO, Sebastian N, de la Fuente MR, Martinez-Garcia JC, Salud J, Perez-Jubindo MA, Diez-Berart S, Dunmur DA, Luckhurst GR. Disentangling molecular motions involved in the

glass transition of a twist-bend nematic liquid crystal through dielectric studies. J Chem Phys 2012 JUL 21;137(3):034502.

37. Robles-Hernandez B, Sebastian N, Rosario de la Fuente M, Lopez DO, Diez-Berart S, Salud J, Ros MB, Dunmur DA, Luckhurst GR, Timimi BA. Twist, tilt, and orientational order at the nematic to twist-bend nematic phase transition of 1 '',9 ''-bis(4-cyanobiphenyl-4 '-yl) nonane: A dielectric, H-2 NMR, and calorimetric study. Physical Review E 2015 DEC 2;92(6):062505.

38. Dunmur D, Luckhurst G, de la Fuente M, Diez S, Jubindo M. Dielectric relaxation in liquid crystalline dimers. J Chem Phys 2001 NOV;115(18):8681-91.

39. Perkowski P. Dielectric spectroscopy of liquid crystals. electrodes resistivity and connecting wires inductance influence on dielectric measurements. Opto-Electronics Review 2012 MAR;20(1):79-86.

40. Perkowski P. Dielectric spectroscopy of liquid crystals. theoretical model of ITO electrodes influence on dielectric measurements. Opto-Electronics Review 2009 JUN;17(2):180-6.

41. Paterson DA, Abberley JP, Harrison WT, Storey JM, Imrie CT. Cyanobiphenyl-based liquid crystal dimers and the twist-bend nematic phase. Liquid Crystals 2017;44(1):127-46.

42. Emsley JW, De Luca G, Lesage A, Merlet D, Pileio G. The structure and conformation of a mesogenic compound between almost zero and almost complete orientational order. Liquid Crystals 2007;34(9):1071-93.

43. Cruickshank E, Salamonczyk M, Pociecha D, Strachan GJ, Storey JMD, Wang C, Feng J, Zhu C, Gorecka E, Imrie CT. Sulfur-linked cyanobiphenyl-based liquid crystal dimers and the twist-bend nematic phase. Liquid Crystals 2019;46(10):1595-609.

44. Adam C, Clark S, Ackland G, Crain J. Conformation-dependent dipoles of liquid crystal molecules and fragments from first principles. Physical Review E 1997 MAY;55(5):5641-9.

45. Borisenko V, Burns D, Zhang Z, Woolley G. Optical switching of ion-dipole interactions in a gramicidin channel analogue. J Am Chem Soc 2000 JUL 12;122(27):6364-70.

46. Ruslim C, Komitov L, Matsuzawa Y, Ichimura K. Effect of conformations of trans- and cis-azobenzenes on photoinduced anchoring transitions in a nematic liquid crystal. Japanese Journal of Applied Physics Part 2-Letters 2000 FEB 1;39(2A):L104-6.

47. Komitov L, Yamamoto J, Yokoyama H. Photoinduced in-plane switching of a photochromic nematic liquid crystal. J Appl Phys 2001 JUN 15;89(12):7730-4.

48. CLARK M, RAYNES E, SMITH R, TOUGH R. Measurement of the permittivity of nematic liquid-crystals in magnetic and electric-fields using extrapolation procedures. Journal of Physics D-Applied Physics 1980;13(11):2151-64.

49. MORRIS S, PALFFYMUHORAY P, BALZARINI D. Measurements of the bend and splay elastic-constants of octylcyanobiphenyl. Molecular Crystals and Liquid Crystals 1986;139(3-4):263-80.

50. Meyer C, Luckhurst GR, Dozov I. Flexoelectrically driven electroclinic effect in the twist-bend nematic phase of achiral molecules with bent shapes. Phys Rev Lett 2013 AUG 6;111(6):067801.

51. Adlem K, Copic M, Luckhurst GR, Mertelj A, Parri O, Richardson RM, Snow BD, Timimi BA, Tuffin RP, Wilkes D. Chemically induced twist-bend nematic liquid crystals, liquid crystal dimers, and negative elastic constants. Physical Review E 2013 AUG 12;88(2):022503.

52. Pociecha D, Crawford CA, Paterson DA, Storey JMD, Imrie CT, Vaupotic N, Gorecka E. Critical behavior of the optical birefringence at the nematic to twist-bend nematic phase transition. Physical Review E 2018 NOV 26;98(5):052706.

53. Stocchero M, Ferrarini A, Moro G, Dunmur D, Luckhurst G. Molecular theory of dielectric relaxation in nematic dimers. J Chem Phys 2004 OCT 22;121(16):8079-97.

54. Balachandran R, Panov VP, Vij JK, Kocot A, Tamba MG, Kohlmeier A, Mehl GH. Elastic properties of bimesogenic liquid crystals. Liquid Crystals 2013 MAY 1;40(5):681-8.

55. Li H, Wen Y, Li P, Wang R, Li G, Ma Y, Yang L, Song Y, Yang Q, Zhu D. A high ON/OFF ratio organic film for photo- and electro-dual-mode recording. Appl Phys Lett 2009 APR 20;94(16):163309.

56. Kumar G, Neckers D. Photochemistry of azobenzene-containing polymers. Chem Rev 1989 DEC;89(8):1915-25.

57. Prasad SK. Photo-stimulated and photo-suppressed phase transitions. Molecular Crystals and Liquid Crystals 2009;509:1059-69.

58. Prasad S, Nair G, Hegde G, Sandhya K, Rao D, Lobo C, Yelamaggad C. Photoinduced effects in nematic liquid crystals. Phase Transitions 2005 JUN;78(6):443-55.

59. Mallia V, Tamaoki N. Photoactive dimesogen having different pathways of light driven phase transitions at different temperatures. Chemical Communications 2004(22):2538-9.

60. Nair G, Prasad S, Hegde G. Influence of a long-chain alkane on the photoinduced nematic-isotropic transition. Physical Review E 2004 FEB;69(2):021708.

61. Paterson DA, Martinez-Felipe A, Jansze SM, Marcelis ATM, Storey JMD, Imrie CT. New insights into the liquid crystal behaviour of hydrogen-bonded mixtures provided by temperature-dependent FTIR spectroscopy. Liquid Crystals 2015;5-6:928-39.

62. Jansze SM, Martinez-Felipe A, Storey JMD, Marcelis ATM, Imrie CT. A twist-bend nematic phase driven by hydrogen bonding. Angewandte Chemie-International Edition 2015 JAN 7 2015;54(2):643-6.

63. Jiang X, Huang W, Zhang S. Flexoelectric nano-generator: Materials, structures and devices. Nano Energy 2013 NOV;2(6):1079-92.

Electronic Supplementary Information

Photo-driven effects in twist-bend nematic phases: dynamic and memory response of liquid crystalline dimers.

Daniel Zaton,[a, b] Alexia Karamoula[a], Grant J. Strachan[b], John M.D. Storey[b], Corrie T. Imrie[b], and Alfonso Martinez-Felipe[a, c,†]

[a.] *Chemical and Materials Engineering Group, School of Engineering, King's College, University of Aberdeen, Aberdeen, AB24 3UE, UK.*
[b.] *Department of Chemistry, King's College, University of Aberdeen, Aberdeen, AB24 3UE, UK.*
[c.] *Centre for Energy Transition, University of Aberdeen, Aberdeen, AB24 3UE, UK.*
† Corresponding author: a.martinez-felipe@abdn.ac.uk

Contents

1. Materials and synthetic procedures.

All the reagents and solvents were purchased from Thermo Fischer Scientific. Inc, or Sigma Aldrich and were used without further purification. CB6OAz(O)n were synthesised following a similar procedure previously reported.[1]

1.1 Synthesis of 6-bromo-1-(4'-bromo-[1,1'-biphenyl]-4-yl) hexan-1-one, BrBK5Br.

A solution of 4- bromobiphenyl (25.05 g, 110 mmol) and 6-bromohexanoyl chloride (24.18 g, 110 mmol in dichloromethane (50 ml) was added dropwise to a stirred suspension of aluminium chloride (14.68 g, 110 mmol) in dichloromethane (50 ml) cooled to 0 °C in an ice bath. This mixture was warmed to room temperature and stirred overnight. The reaction mixture was added to H_2O (250 ml) and extracted using dichloromethane (2 x 80 ml). The organic fraction dried over anhydrous magnesium sulphate before the solvent was removed under vacuum. The crude product was purified by silica gel chromatography (DCM 50%, PE 50%) further recrystallisation from ethanol, to yield the titled compound as a white solid.

30.2 g, 73.6 mmol, 67%. M.P 89 °C. **FT-IR ($\bar{\nu}$, cm^{-1})** 3060, 2938, 1678, 1600, 1512, 1259, 1185, 1076, 1000, 970, 808. **^{1}H NMR (400 MHz, $CDCl_3$)** δ 8.02 (d, *J* = 8.4 Hz, 2H, Ar), 7.64 (d, *J* = 8.4 Hz, 2H, Ar), 7.59 (d, *J* = 8.6 Hz, 2H, Ar), 7.49 (d, *J* = 8.6 Hz, 2H, Ar), 3.44 (t, *J* = 6.7 Hz, 2H, $ArCO(CH_2)_4\underline{CH_2}Br$, 3.02 (t, *J* = 7.3 Hz, 2H, $ArCO\underline{CH_2}(CH_2)_4Br$), 1.98 – 1.88 (m, 2H, $ArCO(CH_2)_3\underline{CH_2}CH_2Br$), 1.84 – 1.75 (m, 2H, $ArCOCH_2\underline{CH_2}(CH_2)_3Br$), 1.59 – 1.50 (m, 2H, $ArCO(CH_2)_2\underline{CH_2}(CH_2)_2Br$). **^{13}C NMR (101 MHz, $CDCl_3$)** δ 199.59, 144.53, 138.88, 136.07, 132.21, 128.95, 128.85, 127.18, 122.76, 38.50, 33.76, 31.07, 28.03, 23.49.

1.2 Synthesis of 4-bromo-4'-(6-bromohexyl)-1,1'-biphenyl, BrB6Br.

Triethylsilane (21.51 g, 185 mmol) was added dropwise to a stirred solution of BrBK5Br (30.1 g, 73.4 mmol) in trifluoroacetic acid (TFA, 64.79 g, 568 mmol) cooled in an ice bath. The reaction mixture was stirred overnight at room temperature and then was added to a mixture of dichloromethane (150 mL) and H_2O (450 mL). The organic layer was extracted and the aqueous phase was washed with dichloromethane (2x150 mL). The organic layer was dried over anhydrous magnesium sulphate and filtered before the solvent was removed under vacuum. The crude product was recrystallized from ethanol to obtain the title product as a white solid.

20.8 g, 52.5 mmol, 72%. M.P 89 °C **FT-IR ($\bar{\nu}$, cm^{-1})** 3031, 2932, 1605, 1479, 1237, 1190, 1079, 1000, 805, 650. **^{1}H NMR (400 MHz, $CDCl_3$)** δ 7.55 (d, *J* = 8.5 Hz, 2H, Ar), 7.46 (t, *J* = 9.1 Hz, 4H, Ar), 7.24 (d, *J* = 8.5 Hz, 2H, Ar), 3.41 (t, *J* = 6.8 Hz, 2H, $Ar(CH_2)_5\underline{CH_2}Br$), 2.66 (t, *J* = 7.7 Hz, 2H, $Ar\underline{CH_2}(CH_2)_5Br$), 1.92 – 1.82 (m, 2H, $ArCH_2CH_2CH_2CH_2\underline{CH_2}CH_2Br$), 1.73 – 1.62 (m, 2H, $ArCH_2\underline{CH_2}CH_2CH_2CH_2CH_2Br$), 1.52 – 1.43 (m, 2H, $ArCH_2CH_2CH_2\underline{CH_2}CH_2CH_2Br$), 1.44 – 1.34 (m, 2H, $ArCH_2CH_2\underline{CH_2}CH_2CH_2CH_2Br$). **^{13}C NMR (101 MHz, $CDCl_3$)**

δ 142.31, 140.17, 137.56, 131.95, 129.10, 128.70, 126.96, 121.35, 35.57, 34.09, 32.87, 31.35, 28.54, 28.16.

1.3 Synthesis of (E)-4-((4-alkyl(oxy)phenyl)diazenyl)phenol, HOAz(O)n.

Concentrated HCl (8,5 mL) and ice (40 g) were added to an ethanol/water solution (1:1, 80 mL) containing the required aniline (1eq) and sodium nitrite (1eq) in an ice bath. Cold water (21 mL) containing phenol (1eq) and NaOH (2eq) was then carefully added to the solution, and the mixture was stirred for 3h. The pH of the solution was adjusted to 1.0 with HCl. The resulting precipitate was filtered, washed with H_2O (400mL) and dried under vacuum. The brown power obtained was recrystallized from hexane to obtain the product as an orange solid.

1.3.1 (E)-4-((4-ethoxyphenyl)diazenyl)phenol, HOAzO2.

8.7 g, 36.0 mmol, 90%. M.P 128 °C. **FT-IR ($\bar{\nu}$, cm^{-1})** 3179, 3034, 2979, 1590, 1501, 1477, 1442, 1385, 1240, 1146, 1116, 1047, 923, 837. **^{1}H NMR (400 MHz, $CDCl_3$)** δ 7.84 (m, 4H, Ar), 6.99 (d, *J* = 8.5 Hz, 2H, Ar), 6.91 (d, *J* = 8.3 Hz, 2H, Ar), 5.54 – 5.49 (s, 1H, OH), 4.11 (q, *J* = 7.0 Hz, 2H, ArO$\underline{CH_2}CH_3$), 1.45 (t, *J* = 7.0 Hz, 3H, ArOCH$_2\underline{CH_3}$). **^{13}C NMR** (101 MHz, $CDCl_3$) δ 161.18, 157.89, 147.32, 146.98, 124.68, 124.51, 115.91, 114.82, 63.96, 14.92.

1.3.2 (E)-4-((4-hexoxyphenyl)diazenyl)phenol HOAzO6.

2.9, 9.7 mmol, 70%. M.P 96 °C. **FT-IR ($\bar{\nu}$, cm^{-1})** 3175, 3046, 2937, 1600, 1583, 1469, 1447, 1380, 1242, 1153, 1106, 1047, 847. **^{1}H NMR** (400 MHz, $CDCl_3$) δ 7.84 (m, 4H, Ar), 6.98 (d, *J* = 8.5 Hz, 2H, Ar), 6.92 (d, *J* = 8.3 Hz, 2H, Ar), 5.52 (s, 1H, OH), 4.03 (t, *J* = 6.7 Hz, 2H, ArO$\underline{CH_2}(CH_2)_4CH_3$) 1.87 – 1.76 (m, 2H, ArOCH$_2\underline{CH_2}(CH_2)_3CH_3$), 1.48 (m, 2H, ArO $CH_2CH_2\underline{CH_2}(CH_2)_2CH_3$), 1.41 – 1.29 (m, 4H, ArO$(CH_2)_3\underline{CH_2CH_2}CH_3$), 0.92 (t, *J* = 6.4 Hz, 3H, ArO$(CH_2)_5\underline{CH_3}$). **^{13}C NMR** (101 MHz, $CDCl_3$) δ 161.39, 157.92, 147.33, 146.96, 124.66, 124.49, 115.91, 114.83, 68.50, 31.73, 29.32, 25.85, 22.75, 14.19.

1.3.3 (E)-4-((4-hexylphenyl)diazenyl)phenol HOAz6.

1.8 g, 6.4 mmol, 30%. M.P 78 °C. **FT-IR ($\bar{\nu}$, cm^{-1})** 3169, 3039, 2937, 1603, 1589, 1471, 1447, 1385, 1242, 1153, 1108, 1047, 836. **^{1}H NMR (400 MHz, $CDCl_3$)** δ 7.85 (d, *J* = 8.6 Hz, 2H, Ar), 7.79 (d, *J* = 8.1 Hz, 2H, Ar), 7.30 (d, *J* = 8.1 Hz, 2H, Ar), 6.92 (d, *J* = 8.6 Hz, 2H, Ar), 5.47 (s, 1H, OH), 2.67 (t, *J* = 7.7 Hz, 2H, Ar$\underline{CH_2}(CH_2)_4CH_3$), 1.71 – 1.60 (m, 2H, ArCH$_2\underline{CH_2}(CH_2)_3CH_3$),), 1.43 – 1.25 (m, 6H, Ar$(CH_2)_2\underline{CH_2CH_2CH_2}CH_3$), 0.89 (t, *J* = 6.4 Hz, 3H, Ar$(CH_2)_5\underline{CH_3}$). **^{13}C NMR** (101 MHz, $CDCl_3$) δ 158.16, 151.04, 147.35, 146.14, 129.21, 124.93, 122.68, 115.92, 36.01, 31.85, 31.43, 29.09, 22.75, 14.24.

1.4 Synthesis of (E)-4'-(6-(4-((4-alkyl(oxy)phenyl)diazenyl)phenoxy)hexyl)-[1,1'-biphenyl]-4-carbonitrile, BrB6OAz(O)n.

A mixture of BrB6Br (1eq), HOAz(O)n (1eq), potassium carbonate (2eq) and dimethylformamide (100 mL) was stirred at reflux overnight. The reaction mixture was cooled to room temperature, poured into H_2O (300 mL), and the orange precipitate was collected by vacuum filtration. The precipitate was dissolved in dichloromethane (150 mL) and washed with H_2O (3 x 50 mL). The organic fraction was dried over anhydrous magnesium sulphate before the solvent was removed under vacuum. The crude product was recrystallized from ethanol/ethyl acetate (2/1) to yield the titled product as an orange solid.

1.4.1 (E)-4'-(6-(4-((4-ethoxy)phenyl)diazenyl)phenoxy)hexyl)-[1,1'-biphenyl]-4-carbonitrile, BrB6OAzO2.

5.8 g, 10.4 mmol, 82%. Cr 156 (N 141) I. **FT-IR ($\bar{\nu}$, cm^{-1})** 3037, 2927, 1603, 1589, 1497, 1479, 1390, 1319, 1245, 1148, 1121, 1044, 1002, 921,837, 807. **^{1}H NMR** (400 MHz, $CDCl_3$) δ 7.86 (d, *J* = 8.6 Hz, 4H, Ar), 7.54 (d, *J* = 8.0 Hz, 2H, Ar), 7.50 – 7.45 (m, 4H, Ar), 7.25 (d, *J* = 8.0 Hz, 2H, Ar), 6.91 (m, 4H, Ar), 4.11 (q, J = 6.9 Hz, 2H, ArO$\underline{CH_2}CH_3$), 4.03 (t, J = 6.4 Hz, 2H, Ar$(CH_2)_5\underline{CH_2}$OAr), 2.67 (t, J = 7.7 Hz, 2H, Ar$\underline{CH_2}(CH_2)_5$OAr), 1.89 – 1.78 (m, 2H, Ar$CH_2CH_2CH_2CH_2\underline{CH_2}CH_2$OAr), 1.75 – 1.65 (m, 2H, Ar$CH_2\underline{CH_2}CH_2CH_2CH_2CH_2$OAr), 1.62 – 1.36 (m, 7H, Ar$CH_2CH_2\underline{CH_2CH_2}CH_2CH_2OAr, ArOCH_2\underline{CH_3}$). **^{13}C NMR** (101 MHz, $CDCl_3$) δ 161.23, 161.09, 147.09, 142.41, 140.15, 137.49, 131.93, 129.10, 128.68, 126.93, 124.45, 121.31, 114.79, 114.78, 68.31, 63.91, 35.60, 31.44, 29.26, 29.08, 26.02, 14.94.

1.4.2 (E)-4'-(6-(4-((4-hexoxy)phenyl)diazenyl)phenoxy)hexyl)-[1,1'-biphenyl]-4-carbonitrile, BrB6OAzO6.

3.6 g, 5.9 mmol, 51%. Cr 147 (N 126) I. **FT-IR ($\bar{\nu}$, cm^{-1})** 3034, 2934, 1602, 1590, 1497, 1479, 1394, 1317, 1242, 1149, 1121, 1047, 999, 921,836, 808. **^{1}H NMR** (400 MHz, $CDCl_3$) δ 7.86 (d, *J* = 8.6 Hz, 4H, Ar), 7.54 (d, *J* = 8.6 Hz, 2H, Ar), 7.45 (m, 4H), 7.24 (d, *J* = 6.9 Hz, 2H, Ar), 7.03 – 6.95 (m, 4H, Ar), 4.03 (t, *J* = 6.4 Hz, 4H, Ar$(CH_2)_5\underline{CH_2}$OAr, ArO$\underline{CH_2}(CH_2)_4CH_3$), 2.67 (t, *J* = 7.7 Hz, 2H, Ar$\underline{CH_2}(CH_2)_5$OAr), 1.91 – 1.77 (m, 4H, Ar$CH_2CH_2CH_2CH_2\underline{CH_2}CH_2OAr, ArOCH_2\underline{CH_2}(CH_2)_3CH_3$), 1.75 – 1.65 (m, 2H, Ar$CH_2\underline{CH_2}CH_2CH_2CH_2CH_2$OAr), 1.59 – 1.32 (m, 10H, Ar$CH_2CH_2\underline{CH_2CH_2}CH_2CH_2OAr, ArO(CH_2)_2\underline{(CH_2)_3}CH_3$), 0.92 (t, *J* = 7.0 Hz, 3H, ArO$(CH_2)_5\underline{CH_3}$). **^{13}C NMR** (101 MHz, $CDCl_3$) δ 161.32, 161.22, 147.10, 147.06, 142.42, 140.16, 137.51, 131.93, 129.11, 128.69, 126.94, 124.44, 121.32, 114.81, 114.80, 68.48, 68.32, 35.60, 31.74, 31.45, 29.34, 29.26, 29.09, 26.03, 25.86, 22.76, 14.20.

1.4.3 (E)-1-(4-((6-(4'-bromo-[1,1'-biphenyl]-4-yl)hexyl)oxy)phenyl)-2-(4-(hexyloxy)phenyl)diazene, Br6OAz6.

2.5 g, 4.2 mmol, 74%. Cr 124 (N 95) I. **FT-IR ($\bar{\nu}$, cm^{-1})** 3038, 2941, 1603, 1589, 1497, 1479, 1390, 1316, 1240, 1147, 1121, 1047, 1003, 923,837, 808. **^{1}H NMR (400 MHz, $CDCl_3$)** δ 7.89 (d, J = 8.8 Hz, 2H, Ar), 7.80 (d, J = 8.2 Hz, 2H, Ar), 7.54 (d, J = 8.4 Hz, 2H, Ar), 7.45 (m, 4H, Ar), 7.30 (d, J = 8.2 Hz, 2H, Ar), 7.25 (m,

2H, Ar), 6.99 (d, J = 8.8 Hz, 2H), 4.04 (t, J = 6.5 Hz, 2H, Ar(CH_2)$_5$$\underline{CH_2}$OAr), 2.67 (t, J = 7.7 Hz, 4H, Ar$\underline{CH_2}$(CH_2)$_5$OAr, Ar$\underline{CH_2}$(CH_2)$_4$$CH_3$), 1.89 – 1.78 (m, 2H, ArCH$_2$CH$_2$CH$_2$CH$_2$$\underline{CH_2}CH_2$OAr), 1.76 – 1.61 (m, 4H, ArCH$_2$$\underline{CH_2}CH_2CH_2CH_2CH_2$OA, ArCH$_2$$\underline{CH_2}$($CH_2$)$_3$$CH_3$), 1.51 – 1.34 (m, 10H, ArCH$_2$CH$_2$$\underline{CH_2}$$\underline{CH_2}CH_2CH_2$OAr, ArCH$_2CH_2$$\underline{(CH_2)_3}$$CH_3$), 0.82 (t, J = 6.6 Hz, 3H, Ar(CH_2)$_5$$\underline{CH_3}$). **^{13}C NMR** (101 MHz, CDCl3) δ 161.54, 151.18, 147.11, 145.96, 142.42, 140.17, 137.53, 131.94, 129.18, 129.11, 128.70, 126.95, 124.70, 122.65, 121.33, 114.81, 68.35, 36.02, 35.61, 31.87, 31.45, 29.26, 29.11, 29.09, 26.03, 22.76, 14.25.

1.5 Synthesis of (E)-4'-(6-(4-((4-alkyl(oxy)phenyl)diazenyl)phenoxy)hexyl)-[1,1'-biphenyl]-4-carbonitrile, CB6OAz(O)n.

A Rosemund – von Braun reaction was used in the synthesis of CB6OAz(O)n.[2] A mixture of BrBC6OAzO2 (1eq), copper cyanide (2eq) and dry N-methyl-2-pyrrolidone (25 ml) was heated to 200 °C for 6 h. The reaction mixture was cooled to 80 °C and to this was added a solution of iron chloride (16.0 g, 98.9 mmol), H_2O (137eq) and 32 % hydrochloric acid (10eq) at 60 °C. This was allowed to cool slowly to room temperature and stirred overnight, then added to a dichloromethane (200 ml) and H_2O (200 ml) mix. The aqueous layer was washed with dichloromethane (100 ml). The organic fraction was dried over anhydrous magnesium sulphate and filtered before the solvent was dried under vacuum. The crude oil obtained was added into H_2O and the precipitate was filtered under vacuum. The crude product was purified by silica gel chromatography using dichloromethane as eluent. The crude product thus obtained was recrystallized from ethanol to give the title compound as an orange solid.

1.5.1 (E)-4'-(6-(4-((4-ethoxyphenyl)diazenyl)phenoxy)hexyl)-[1,1'-biphenyl]-4-carbonitrile, CB6OAzO2, 3 (Fig. ESI1 to ESI3)

2.5g, 5.0 mmol, 50%. Cr 99.9 Cr 136.3 (N_{TB} 113.2) N 168.0 I. **FT-IR ($\bar{\nu}$, cm^{-1})** 3063, 2962, 2224, 1600, 1589, 1497, 1474, 1395, 1320, 1253, 1148, 1023, 1000, 837, 809. **^{1}H NMR** (400 MHz, $CDCl_3$) δ 7.86 (dd, *J* = 9.0, 2.8 Hz, 4H, Ar), 7.68 (q, *J* = 8.3 Hz, 4H, Ar), 7.50 (d, *J* = 7.8 Hz, 2H, Ar), 7.29 (d, *J* = 7.8 Hz, 2H, Ar), 7.02 – 6.94 (m, 4H, Ar), 4.12 (q, *J* = 7.0 Hz, 2H, ArO$\underline{CH_2}$$CH_3$), 4.03 (t, *J* = 6.4 Hz, 2H, Ar(CH_2)$_5$$\underline{CH_2}$OAr), 2.69 (t, *J* = 7.7 Hz, 2H, Ar$\underline{CH_2}$(CH_2)$_5$OAr), 1.89 – 1.79 (m, 2H, ArCH$_2$CH$_2$CH$_2$CH$_2$$\underline{CH_2}CH_2$OAr), 1.77 – 1.65 (m, 2H, ArCH$_2$$\underline{CH_2}CH_2CH_2CH_2CH_2$OAr), 1.59 – 1.39 (m, 7H, ArCH$_2$CH$_2$$\underline{CH_2}$$\underline{CH_2}CH_2CH_2$OAr, ArOCH$_2$$\underline{CH_3}$). **^{13}C NMR (101 MHz, $CDCl_3$)** δ 161.22, 161.13, 147.11, 147.10, 145.70, 143.73, 136.66, 132.71, 129.32, 127.62, 127.23, 124.43, 119.09, 114.76, 110.68, 68.27, 63.92, 35.61, 31.38, 29.25, 29.03, 26.01, 14.95. **EA** calculated for $C_{33}H_{33}N_3O_2$: C, 78.70%, H, 6.60%, N, 8.34%, O, 6.35%. Found: C, 78.71%, H, 6.41%, N, 8.34%, O, 6.54%.

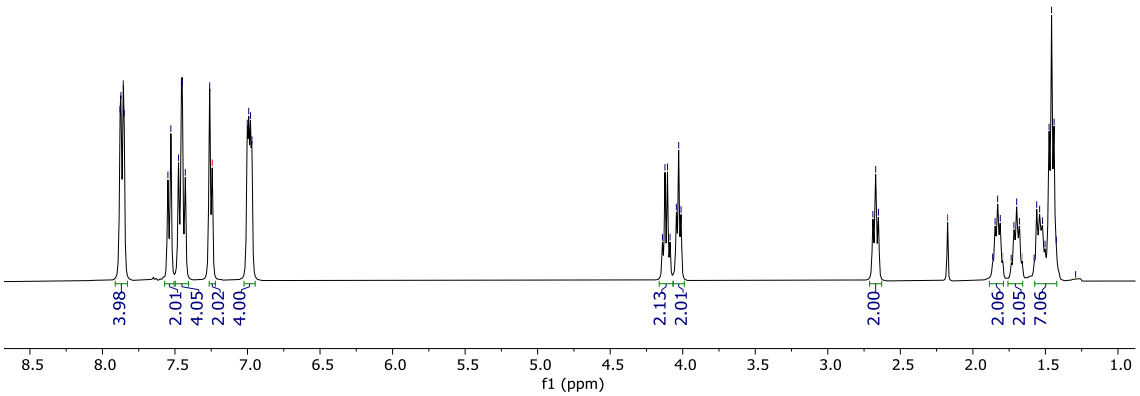

Fig. ESI1. ^{1}H-NMR spectrum of CB6OAzO2.

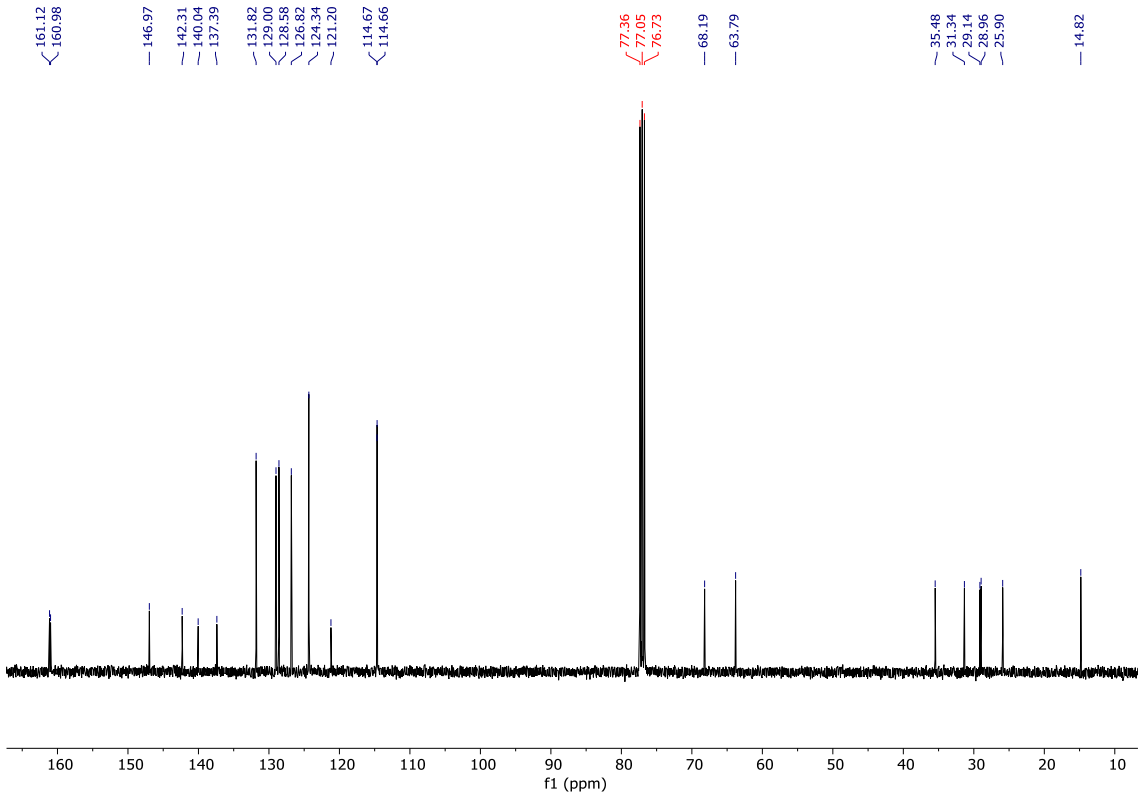

Fig. ESI2. ^{13}C-NMR spectrum of CB6OAzO2.

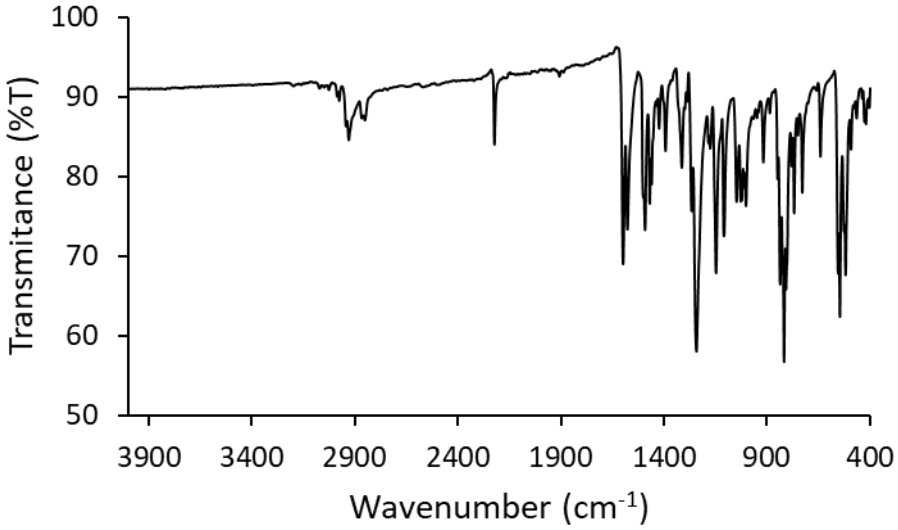

Fig. ESI3. ATR-IR spectrum of CB6OAzO2.

1.5.2 (E)-4'-(6-(4-((4-(hexyloxy)phenyl)diazenyl)phenoxy)hexyl)-[1,1'-biphenyl]-4-carbonitrile, CB6OAzO6, 4 (Fig. ESI4 to ESI6).

0.9 g, 1.6 mmol, 29%. Cr 108.7 Cr 123.6 (N_{TB} 97.6) N 143.0 I. **FT-IR ($\bar{\nu}$, cm^{-1})** 3065, 2962, 2228, 1603, 1578, 1497, 1472, 1395, 1319, 1240, 1143, 1027, 1002, 839, 817. **^{1}H NMR (400 MHz, $CDCl_3$)** δ 7.87 (dd, *J* = 8.9, 2.1 Hz, 4H, Ar), 7.68 (q, *J* = 8.2 Hz, 4H, Ar), 7.50 (d, *J* = 7.8 Hz, 2H), 7.29 (d, *J* = 7.8 Hz, 2H), 6.99 (t, *J* = 8.6, 4H, Ar), 4.03 (t, *J* = 6.7 Hz, 4H, $Ar(CH_2)_5\underline{CH_2}OAr$, $ArO\underline{CH_2}(CH_2)_4CH_3$), 2.69 (t, *J* = 7.7 Hz, 2H, $Ar\underline{CH_2}(CH_2)_5OAr$), 1.89 – 1.77 (m, 4H, $ArCH_2CH_2CH_2CH_2\underline{CH_2}CH_2OAr$), 1.76 – 1.67 (m, 2H, $ArCH_2\underline{CH_2}CH_2CH_2CH_2CH_2OAr$), 1.61 – 1.33 (m, 2H, 10H, $ArCH_2CH_2\underline{CH_2CH_2}CH_2CH_2OAr$, $ArO(CH_2)_2\underline{(CH_2)_3}CH_3$), 0.93 (t, *J* = 7.0 Hz, 3H, $ArO(CH_2)_5\underline{CH_3}$). **^{13}C NMR** (101 MHz, $CDCl_3$) δ 161.33, 161.18, 147.09, 147.02, 145.66, 143.60, 136.63, 132.67, 129.31, 127.58, 127.21, 124.42, 119.16, 114.79, 114.77, 110.66, 68.46, 68.25, 35.60, 31.71, 31.35, 29.32, 29.22, 29.02, 25.99, 25.84, 22.74, 14.18. **EA** calculated for $C_{37}H_{41}N_3O_2$: C, 79.39%, H, 7.38%, N, 7.51%, O, 5.72%. Found: C, 79.48%, H, 7.47%, N, 7.4%, O, 5.65%.

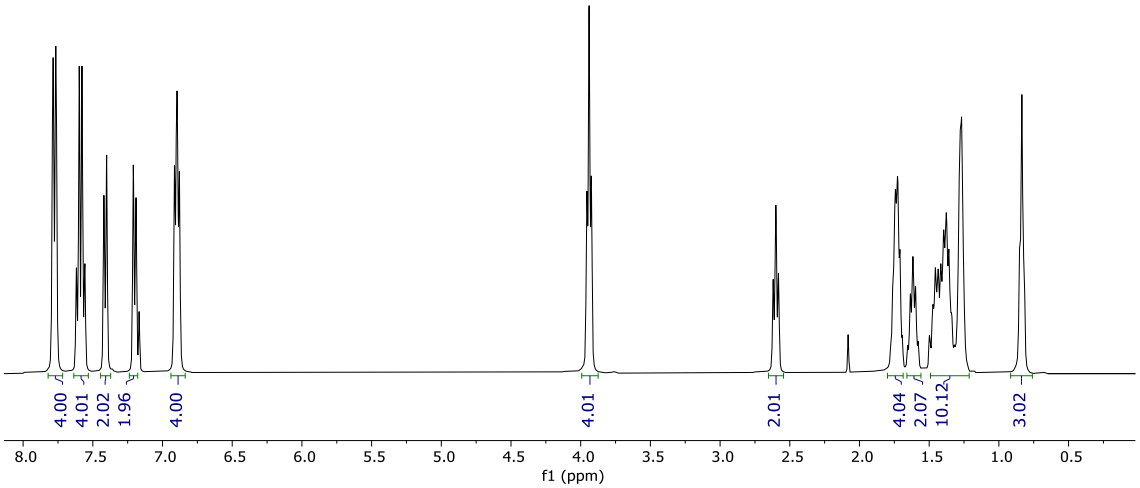

Fig. ESI4. ^{1}H-NMR spectrum of CB6OAzO6.

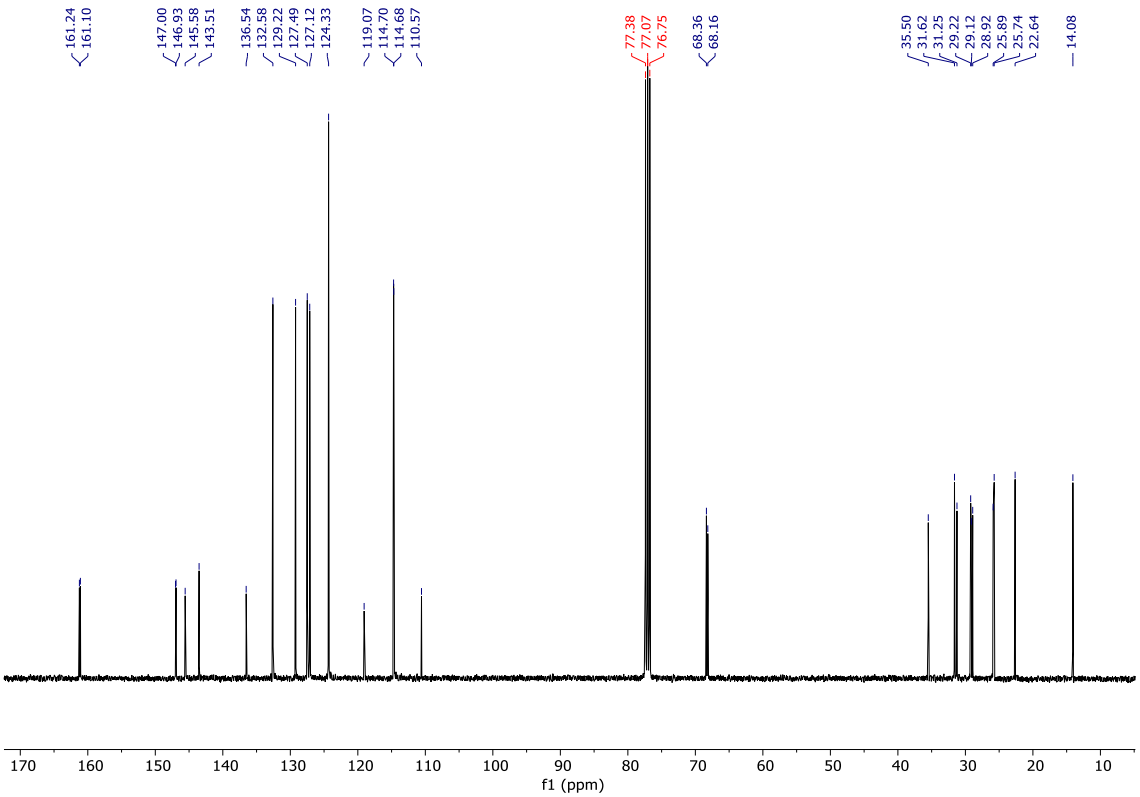

Fig. ESI5. ^{13}C-NMR spectrum of CB6OAzO6.

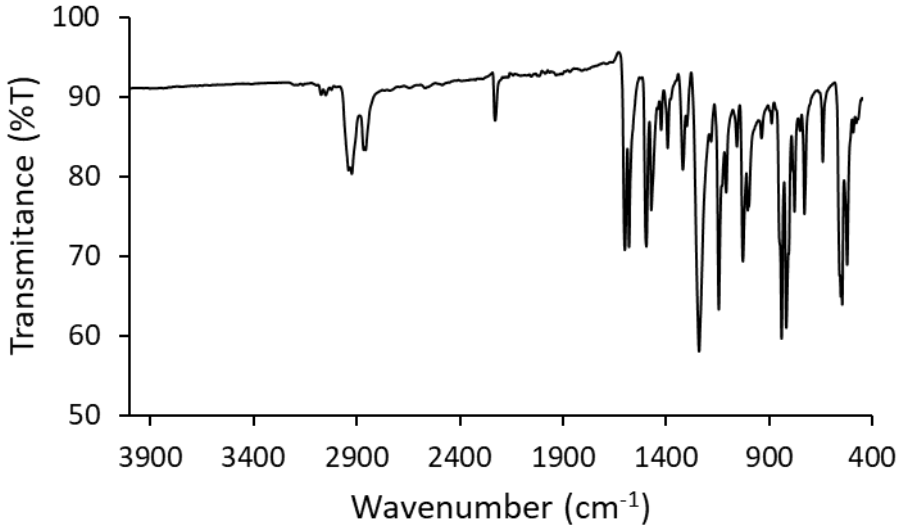

Fig. ESI6. ATR-IR spectrum of CB6OAzO6.

1.5.3 (E)-4'-(6-(4-((4-hexylphenyl)diazenyl)phenoxy)hexyl)-[1,1'-biphenyl]-4-carbonitrile, CB6OAz6, 5 (Fig. ESI7 to ESI9).

0.7 g, 1.3 mmol, 30%. Cr 84.7 (N_{TB} 79.1) N 118.4 I. **FT-IR ($\bar{\nu}$, cm^{-1})** 3065, 2962, 2227, 1600, 1578, 1497, 1472, 1395, 1319, 1240, 1143, 1027, 1002, 839, 817. **^{1}H NMR** (400 MHz, $CDCl_3$) δ 7.89 (d, *J* = 8.1 Hz, 2H, Ar), 7.80 (d, *J* = 8.1 Hz, 2H, Ar), 7.69 (q, *J* = 7.7 Hz, 4H, Ar), 7.50 (d, *J* = 7.8 Hz, 2H, Ar), 7.34 – 7.24 (m, 4H, Ar), 6.99 (d, J = 8.1 Hz, 2H, Ar), 4.04 (t, J = 6.4 Hz, 2H, $Ar(CH_2)_5\underline{CH_2}OAr$), 2.69 (q, *J* = 7.2 Hz, 4H, $Ar\underline{CH_2}(CH_2)_5OAr$, $Ar\underline{CH_2}(CH_2)_4CH_3$), 1.83 – 1.70 (m, 2H, $ArCH_2CH_2CH_2CH_2\underline{CH_2}CH_2OAr$), 1.70 – 1.53 (m, 4H, $ArCH_2\underline{CH_2}CH_2CH_2CH_2CH_2OA$, $ArCH_2\underline{CH_2}(CH_2)_3CH_3$), 1.52 – 1.25 (m, 10H, $ArCH_2CH_2\underline{CH_2CH_2}CH_2CH_2OAr$, $ArCH_2CH_2\underline{(CH_2)_3}CH_3$), 0.82 (t, J = 6.4 Hz, 3H, $Ar(CH_2)_5\underline{CH_3}$).**^{13}C NMR** (101 MHz, $CDCl_3$) δ 161.50, 151.15, 147.10, 145.98, 145.69, 143.62, 136.66, 132.69, 129.32, 129.18, 127.60, 127.24, 124.68, 122.64, 119.17, 114.79, 110.68, , 68.30, 36.01, 35.62, 31.85, 31.44, 31.37, 29.23, 29.10, 29.03, 26.00, 22.75, 14.24. **EA** Calculated for $C_{37}H_{41}N_3O$: C, 81.73%, H, 7.60%, N, 7.73%, O, 2.94%. Found: C, 81.55%, H, 7.62%, N, 7.59%, O, 3.24%.

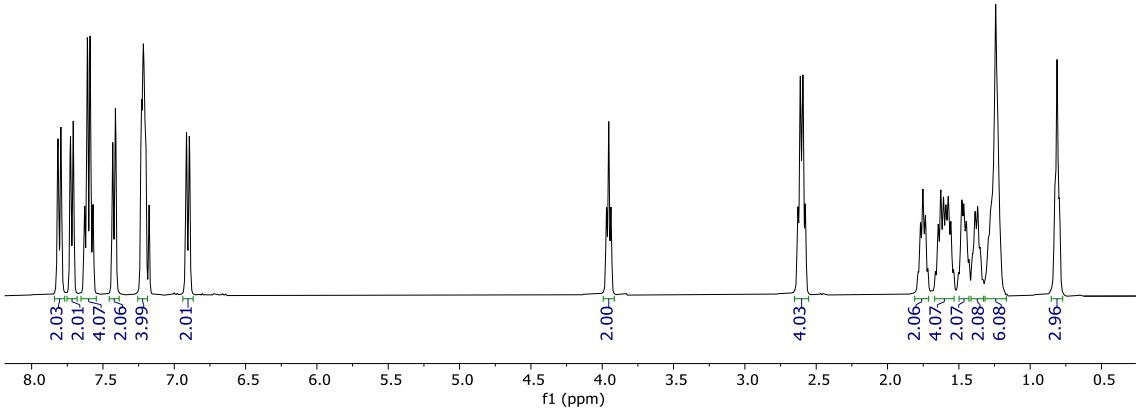

Fig. ESI7. ^{1}H-NMR spectrum of CB6OAz6.

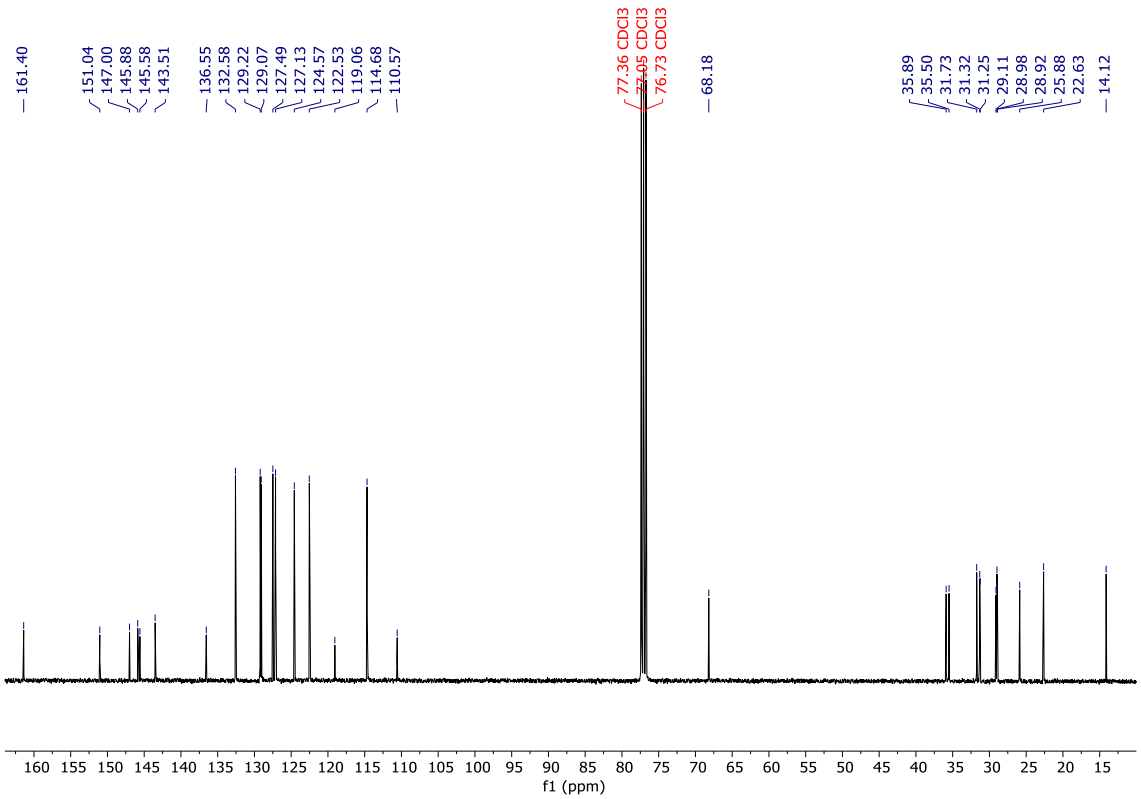

Fig. ESI8. ^{13}C-NMR spectrum of CB6OAz6.

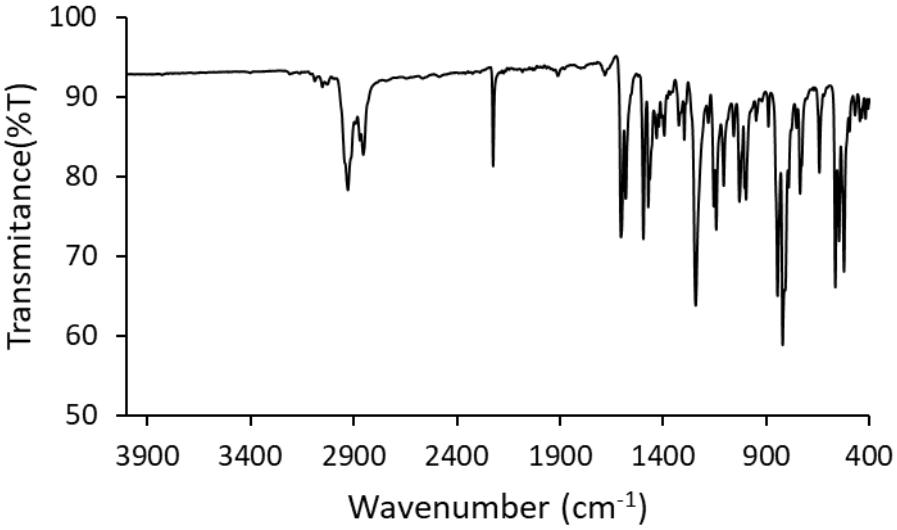

Fig. ESI9. ATR-IR spectrum of CB6OAz6.

2. Differential scanning calorimetry, DSC, thermograms.

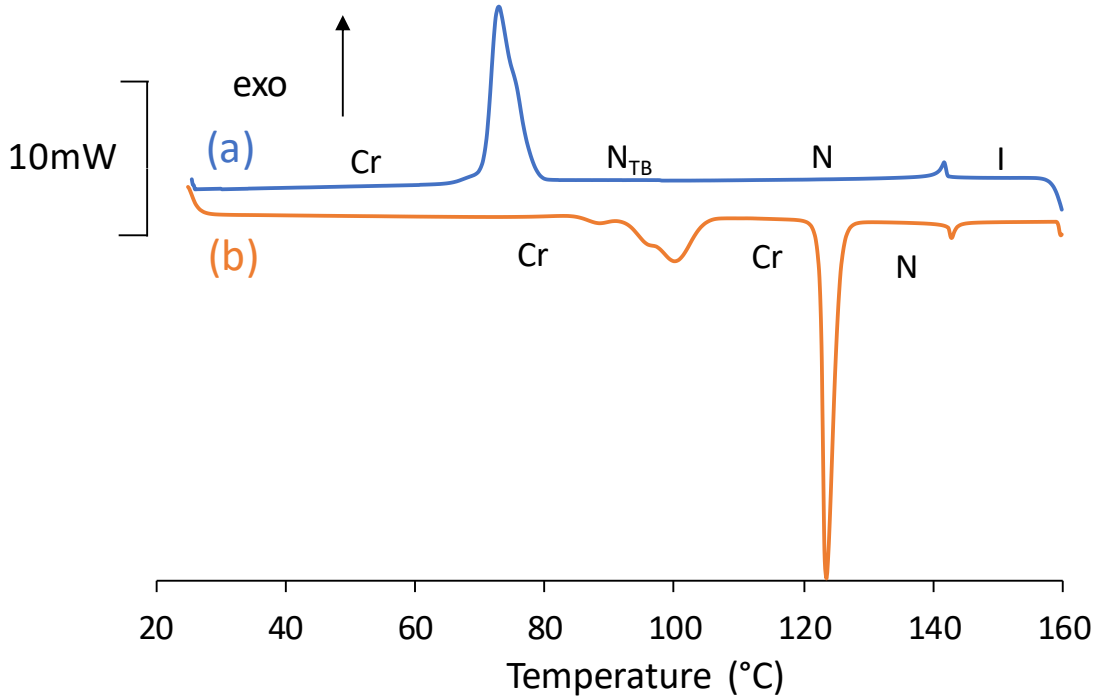

Fig. ESI10. Differential scanning calorimetry, DSC, thermograms, for CB6OAzO6, obtained during the cooling scan (a) and second heating scan (b).

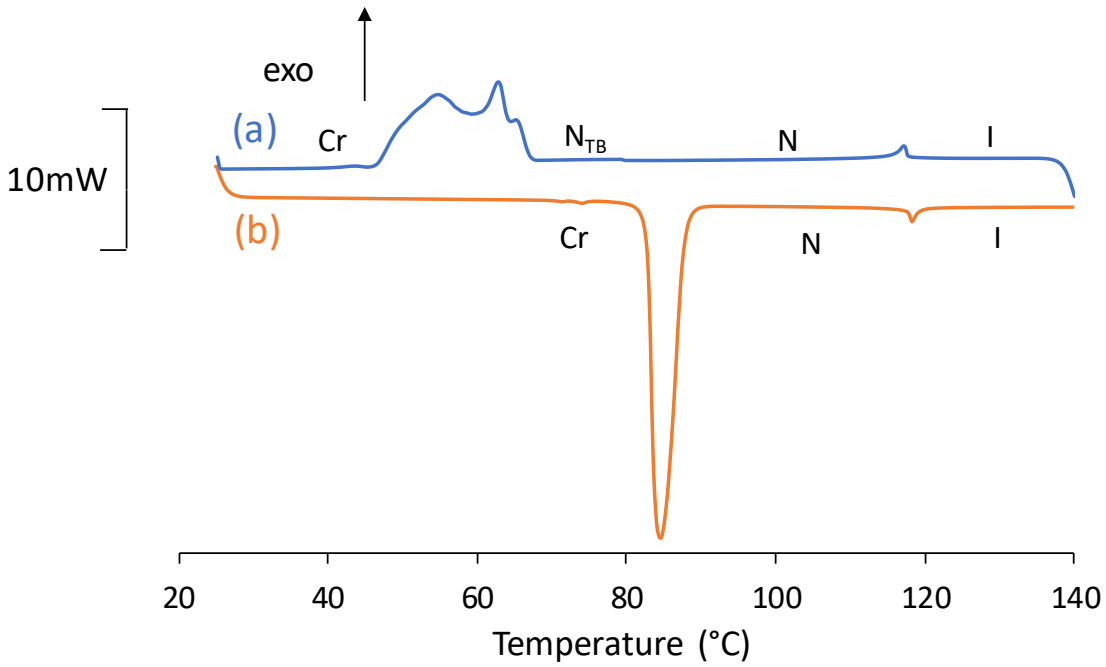

Fig. ESI11. Differential scanning calorimetry, DSC, thermograms, for CB6OAz6, obtained during the cooling scan (a) and second heating scan (b).

3. Dielectric response.

The splay, K_1, and bend, K_3, elastic constants in the nematic phase were determined by measuring the dielectric permittivity change under increasing ac fields of 0 to 20 Vrms, at 5 kHz. Measurements were performed over the temperature range of the nematic phase, using 8 µm glass cells with transparent indium tin oxide (ITO) electrodes. For each temperature the capacitance of the cell as a function of the applied amplitude voltage was plotted (V_{rms}). The splay elastic constant K_1 was determined from the threshold voltage V_{th} at which the director reorientation starts, and thus the permittivity starts to increase as:

$$K_1 = \Delta\varepsilon \times 8 \cdot 85 \times \left(\frac{V_{th}^2}{\pi^2}\right)$$

The bend elastic constant, K_3 was estimated by fitting the $\varepsilon'(V^{-1})$ curve to the following expression,

$$\left(\frac{\varepsilon(V) - \varepsilon_\perp}{\varepsilon_{II} - \varepsilon_\perp}\right) = \left(1 - \frac{2}{\pi}(1+\gamma)^{1/2}\right)\frac{V_{th}}{V}c$$

where $\gamma = (\varepsilon_{II} - \varepsilon_\perp)/\varepsilon_\perp$, above the threshold voltage [31], in the linear regime of the curve fitting dependence.

The fitting provides the constant C, which takes the value of the integral:

$$\int_0^1 \left(\frac{1 + (\frac{k_{33}}{k_{11}})x^2}{1 + \gamma x^2}\right)^{\frac{1}{2}} \cdot dx$$

The value of the bend elastic constant, K_3, was then estimated by adjusting the integral numerically, using Solver.

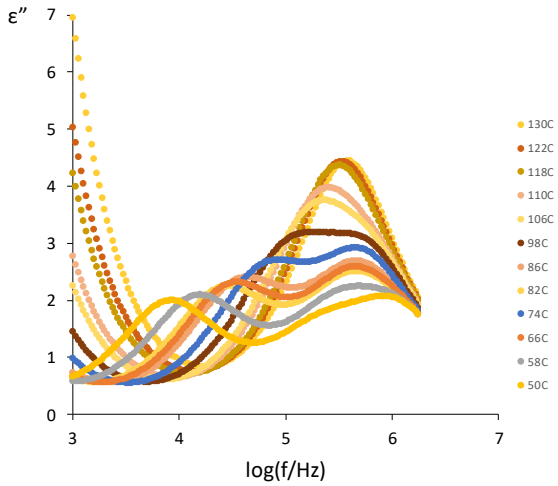

Fig. ESI12. Dielectric loss factor, ε'', measured for CB6OAz6 on cooling from the isotropic phase to the twist-bend nematic phase. Results obtained in the presence of a strong alternating electric field (V_{rms}=19 V). T_{NTBN} = 67.5 °C, T_{NI} = 122.5 °C.

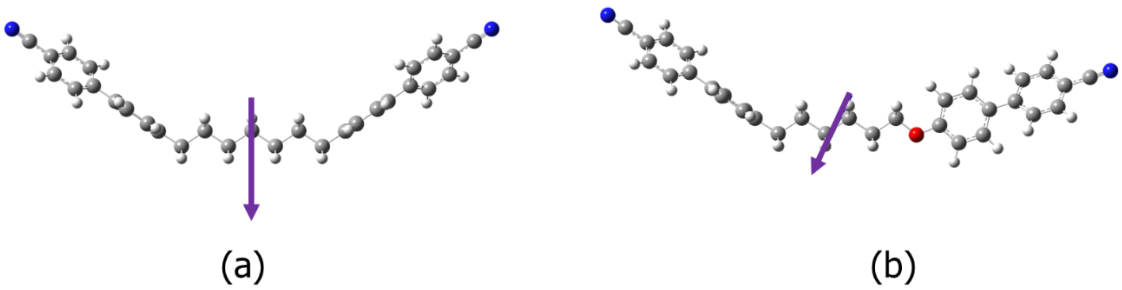

Fig. ESI13. Ball-and-stick models of (a) 1,7-bis(4-cyanobiphenyl-4-yl) heptane , CB7CB, and (b) 4'-((6-(4'-cyano-[1,1'-biphenyl]-4-yl)hexyl)oxy)-[1,1'-biphenyl]-4-carbonitrile, CB6OCB, corresponding to their optimised molecular geometries obtained by Density Functional Theory, DFT. Arrows indicate the direction of their molecular dipoles (6.4378 D and 4.6135 D, respectively).

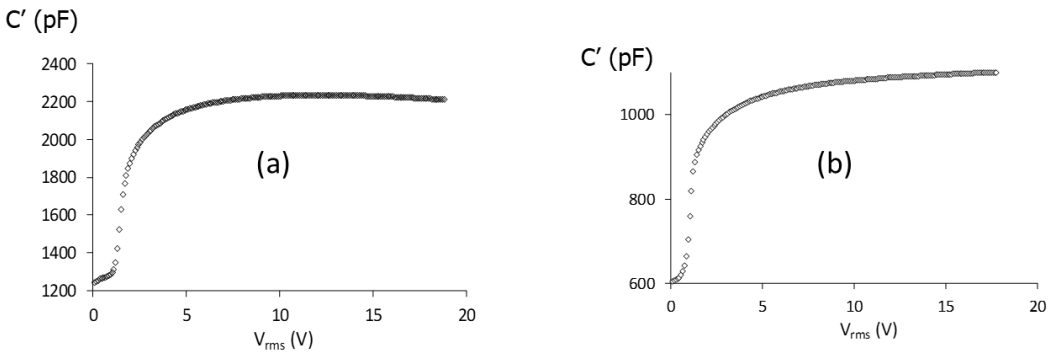

Fig. ESI14. (a) Capacitance, C' , as a function of the voltage (V_{rms}) for (a) CB6OAzO6 and (b) CB6OAz6, obtained in their nematic phases (T=160 °C and T=104 °C, respectively).

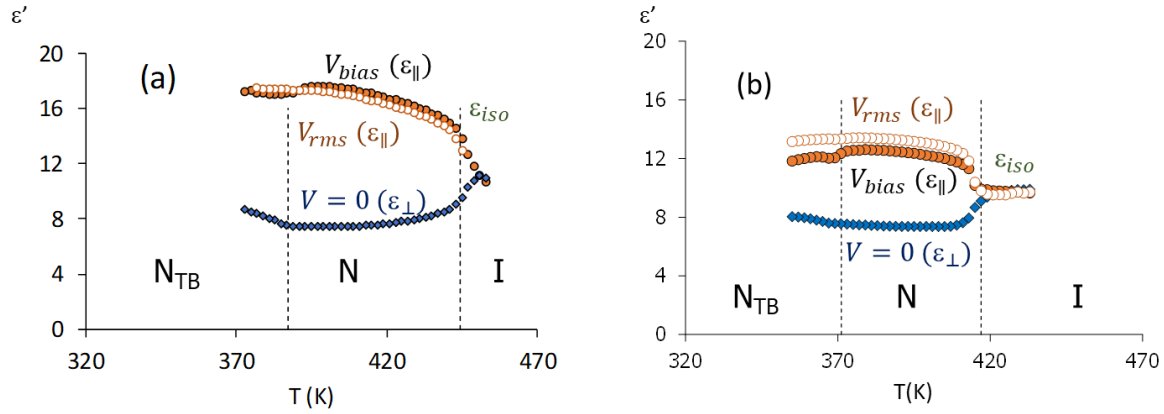

Fig. ESI15. Components of the dielectric elastic constant, ε', in isothermal steps on cooling from the isotropic phase, I (ε_{iso}), through the nematic phase, N, to the twist-bend nematic phase, N_{TB}: perpendicular V=0 ($\varepsilon_{\perp}$) and parallel with V_{bias} = 35 V and V_{rms} = ± 19 V: (a) CB6OAzO2; (b) CB6OAzO6. Vertical dotted lines show the respective T_{NI} and T_{NTBN} phase transitions.

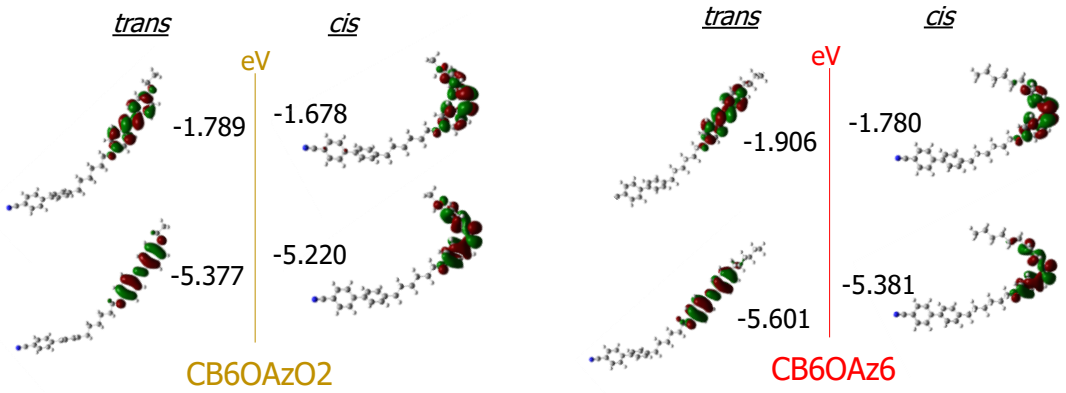

Figure ESI16. Balls-and-sticks models corresponding to the *trans* and *cis* isomers of the CB6OAzO2 (left) and CB6OAz6 (right) dimers after optimization by DFT, including their respective highest occupied and lowest unoccupied molecular orbital energy levels (HOMO and LUMO, respectively), and their electrostatic configurations.

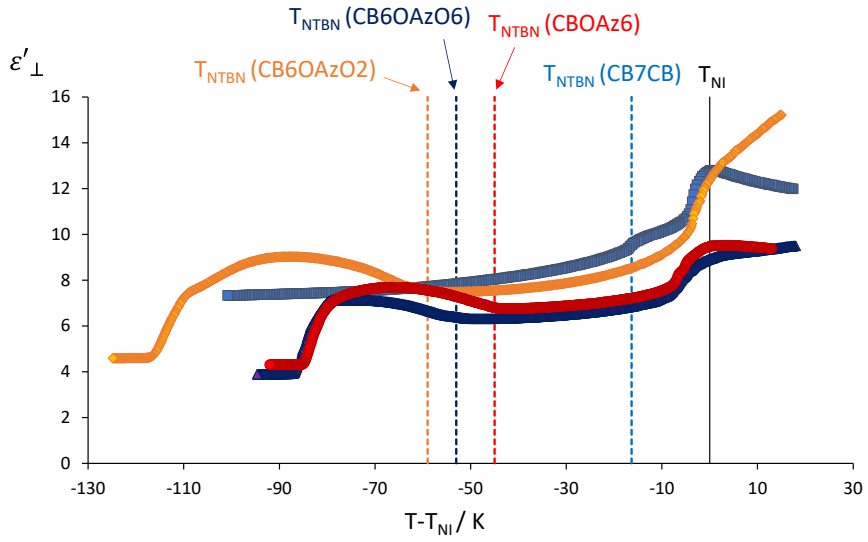

Fig. ESI17. Static dielectric elastic constant, ε' (5 KHz) measured in isothermal steps on cooling from the isotropic to the twist-bend nematic phase, in planar cells (V=0), as a function of reduced temperature respect to the nematic to isotropic transition, $T - T_{NI}$: (◇) CB6OAzO2, (▲) CB6OAzO6, (●) CB6OAz6 and (□) CB7CB. Dotted lines indicate the respective twist-bend nematic to nematic transitions, T_{NTBN}.

4. Light-responsive behaviour.

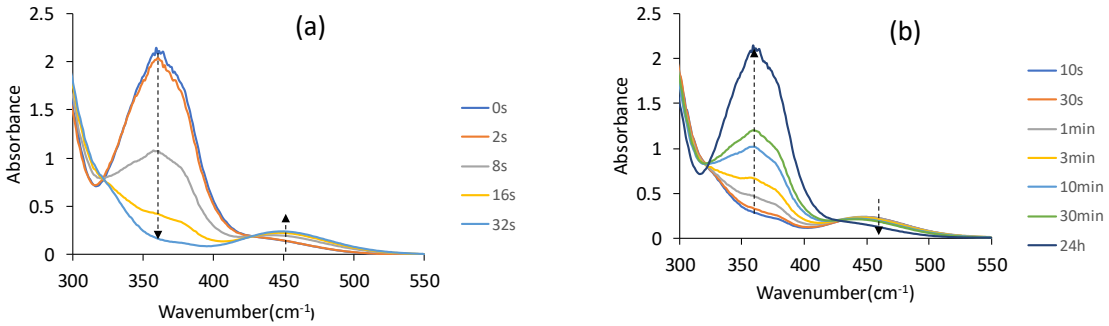

Fig. ESI18. (a) UV-Vis spectra of CB6OAzO2 measured in THF solution (3 10^{-5} M) at different irradiation times, showing a dramatic decrease in intensity π–π* transition and a simultaneous though less marked increase of the n–π* transition band. (b) UV spectra of CB6OAzO2 after UV_{off} at different times, observing the opposite effect in the absorption bands.

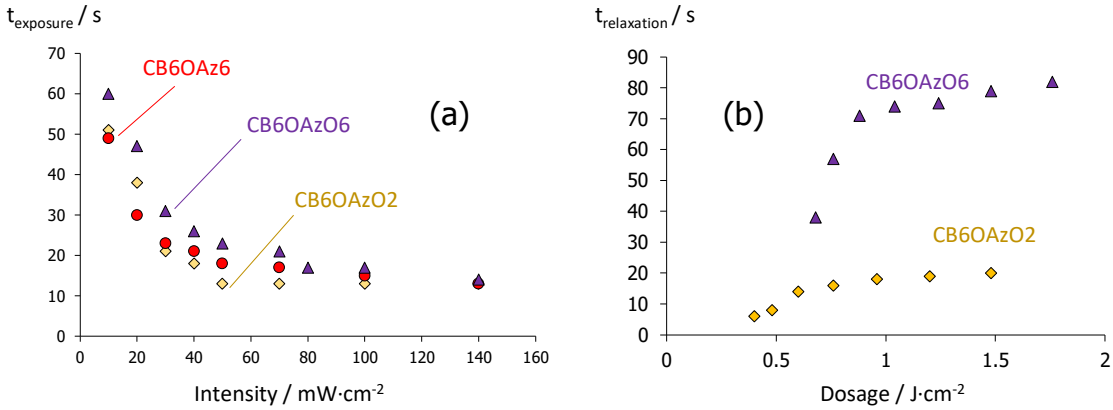

Fig. ESI19. (a) Exposure time required to drive the N_{TB} to N isothermal phase transition, and (b) time required for the back N to N_{TB} relaxation, for the dimers, and as a function of UV dosage at T-T_{NNTB} = - 5 K. (◇) CB6OAzO2, (▲) CB6OAzO6 and (●) CB6OAz6.

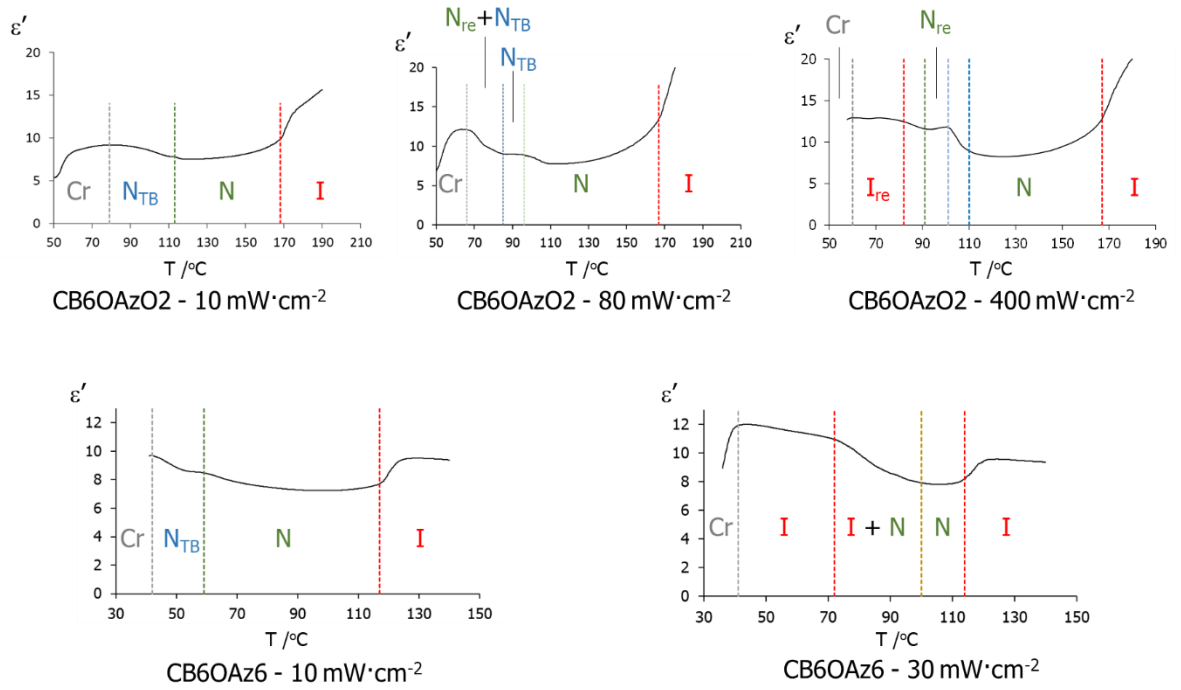

Fig. ESI20. Examples of the static dielectric elastic constant, ε' (5 kHz), measured on cooling at 2 °C·min^{-1} from the isotropic to the crystal phases, in planar cells (V = 0), showing transitions between: isotropic (I), nematic (N), twist-bend nematic (N_{TB}), re-entrant isotropic (I_{re}) and nematic (N_{re}) phases. Not all biphasic regions are shown for the sake of clarity.

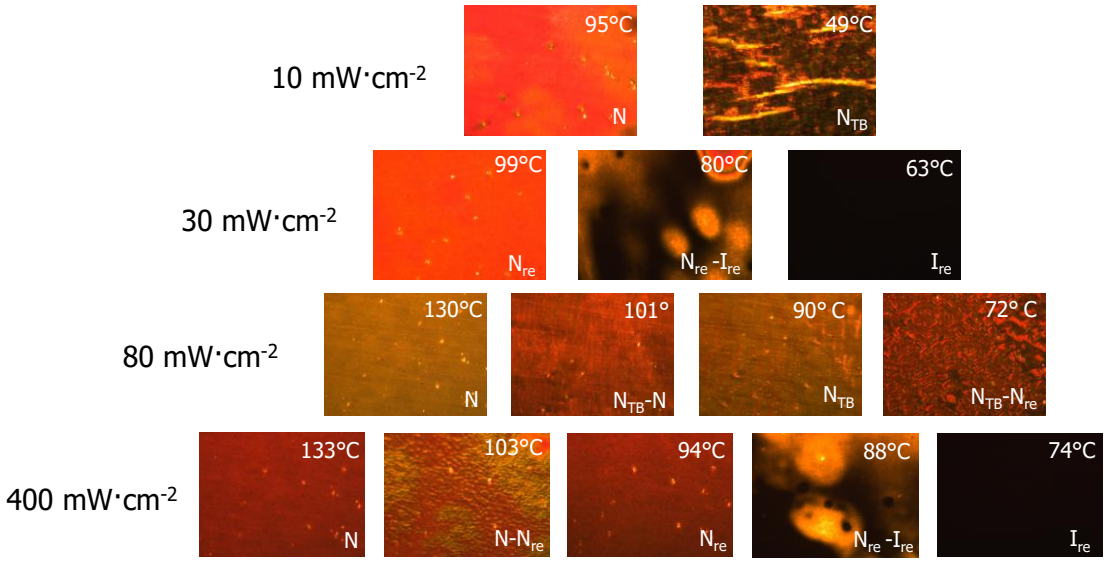

Fig. ESI21. Optical textures of the phases and biphasic regions observed for: CB6OAz6 (10 and 30 mW·cm^{-2}) and CB6OAzO2 (80 and 400 mW·cm^{-2}), under different UV intensities, corresponding to the experiments shown in Fig. ESI20.

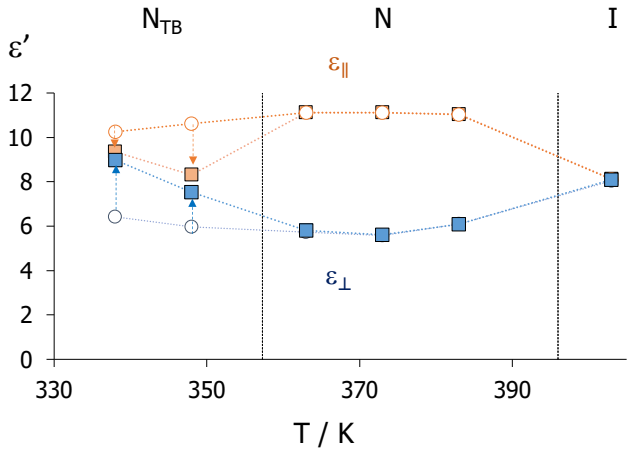

Fig. ESI22. Temperature dependence of the static dielectric permittivity (5 kHz) of CB6OAz6 measured in planar cells in the absence ($\boldsymbol{\varepsilon}_{\perp}$) and presence of V_{bias} = 35V ($\boldsymbol{\varepsilon}_{\parallel}$) : before UV exposure (empty circles) and after UV exposure (120 mW·cm^{-2}) and relaxation for ten minutes (full squares). Vertical lines indicate twist-bend nematic (N) to nematic (N), and nematic to isotropic (I) transitions. Values during UV exposure have been omitted for the sake of clarity.

5. References

(1) Paterson, D. A.; Xiang, J.; Singh, G.; Walker, R.; Agra-Kooijman, D. M.; Martínez-Felipe, A.; Gao, M.; Storey, J. M. D.; Kumar, S.; Lavrentovich, O. D.; Imrie, C. T. Reversible Isothermal Twist-Bend Nematic-Nematic Phase Transition Driven by the Photoisomerization of an Azobenzene-Based Nonsymmetric Liquid Crystal Dimer. *J. Am. Chem. Soc.* **2016**.

(2) Coates, D.; Gray, G. W. Properties of the Liquid Crystals Formed by Some 4'-Substituted 4-(β-p-Substituted Arylethyl)Biphenyls. *J. Chem. Soc. Perkin Trans. 2* **1976**.

(3) T. Uchida and Y. Takahashi, "New Method to Determine Elastic Constants of Nematic Liquid Crystal From C-V Curve," Molecular Crystals and Liquid Crystals, vol. 72, no. 4, pp. 133-137, 2007.